INT PROGRAM INT-23-1A

Intersection of nuclear structure and high-energy nuclear collisions

January 23, 2023 - February 24, 2023

Accessing structure of protons and nuclei at small x at the Electron-Ion Collider

Wenbin Zhao

Wayne State University, Brookhaven National Laboratory

Collaborators: Heikki Mäntysaari, Björn Schenke, and Chun Shen

Feb. 24, 2023, INT workshop

Hydrodynamics response to collision geometry

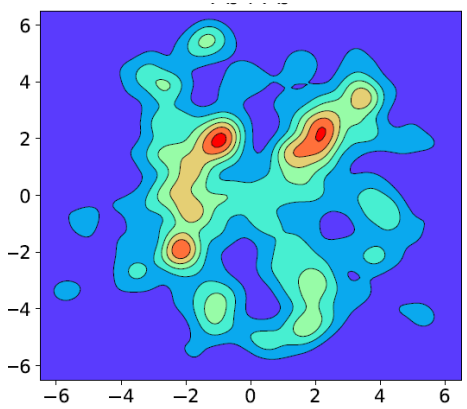

Hydrodynamics

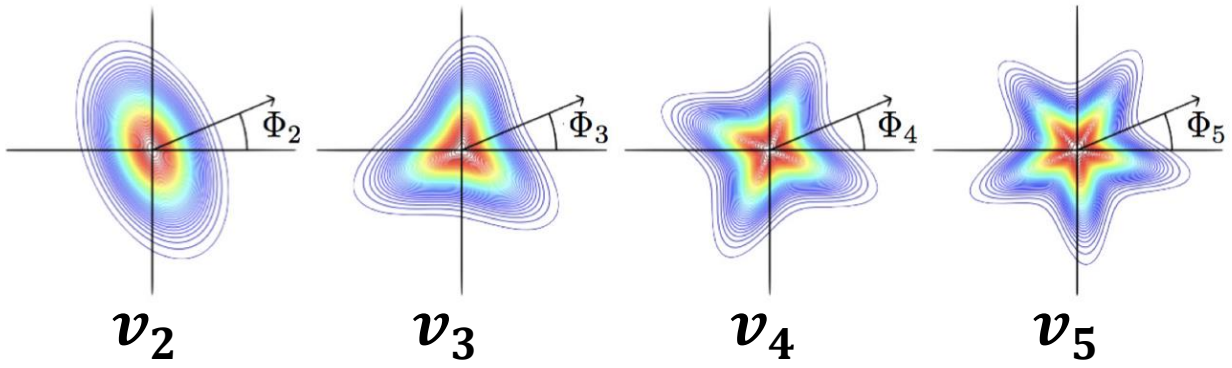

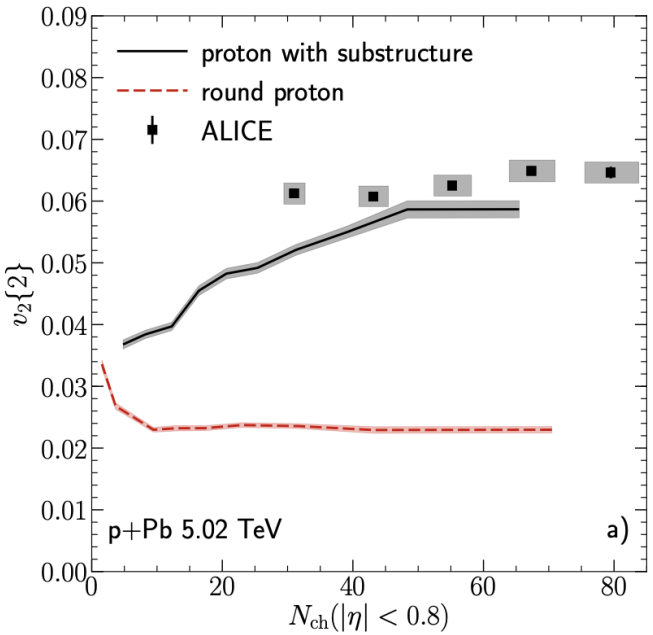

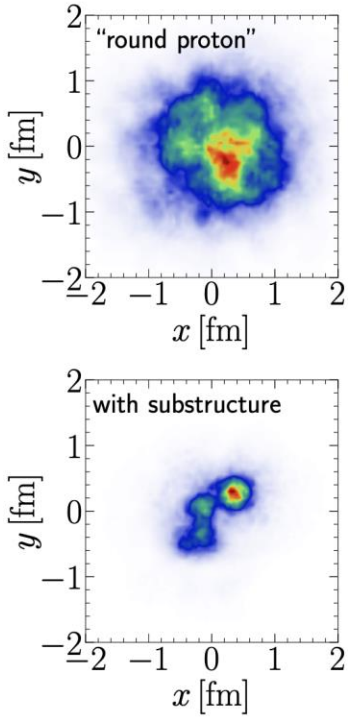

- Heavy-ion Collisions: Initial spatial geometry ⇒ final momentum anisotropy.
- Proton's sub-nucleonic structure is crucial to understand the collectivity in small collision systems

B. Schenke, Rept. Prog. Phys. 84, 082301 (2021).

Diffraction in optics

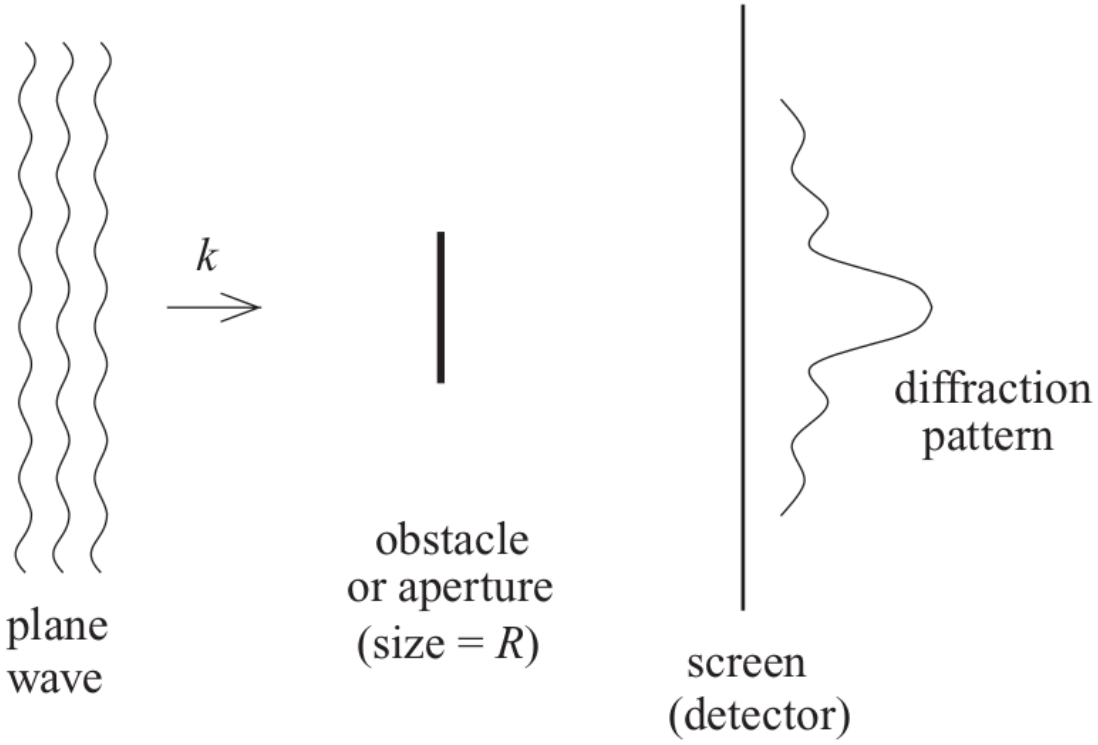

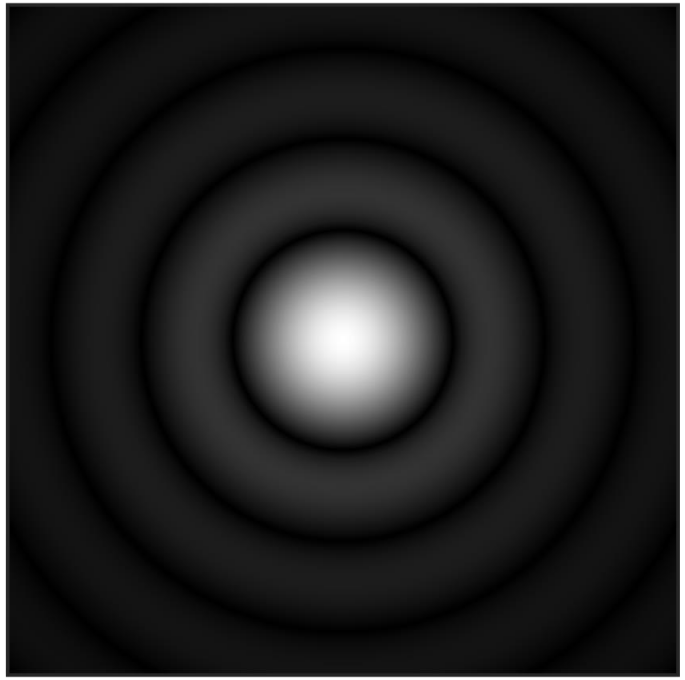

Taken from Wiki

- In momentum-space the positions of the minima and maxima of diffraction pattern are determined solely by the target size R.

Constrain fluctuating proton geometry from DIS

Diffractive vector meson production

High energy factorization:

1. $\gamma^* \to q\bar{q}$ splitting, wave function $\Psi^\gamma(r, Q^2, z)$
2. $q\bar{q}$ dipole scatters elastically
3. $q\bar{q} \to J/\Psi$, wave function $\Psi^V(r, Q^2, z)$

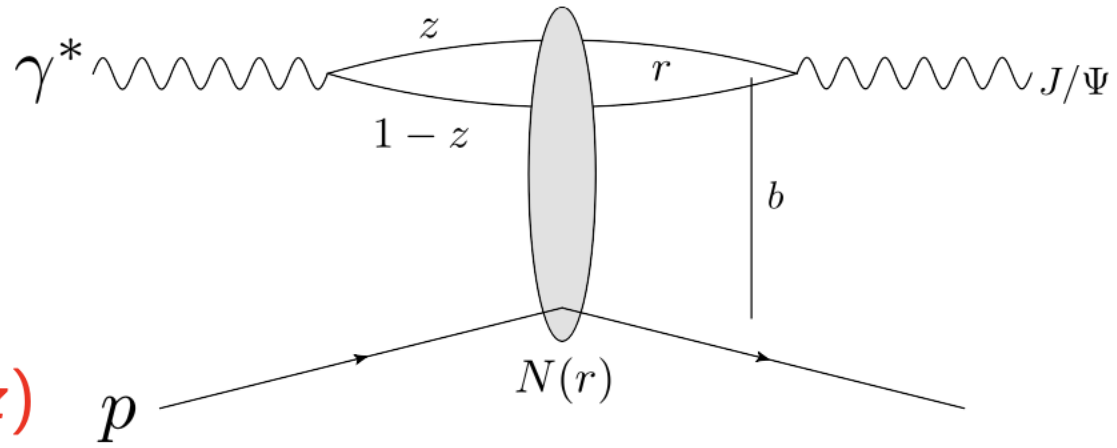

Diffractive scattering amplitude

$$\mathcal{A}^{\gamma^* p \to Vp} \sim \int \mathrm{d}^2 b \mathrm{d}z \mathrm{d}^2 r \Psi^{\gamma *} \Psi^V(r, z, Q^2) \mathbf{e}^{-\mathbf{ib}\cdot\mathbf{\Delta}} N(r, x, b)$$

Impact parameter, b, is the Fourier conjugate of the momentum transfer, $\Delta \approx \sqrt{-t}$

N(r, x, b) dipole-target scattering amplitude.

Miettinen, Pumplin, PRD 18, 1978; Caldwell, Kowalski, 0909.1254; Mäntysaari, Schenke, 1603.04349; Mäntysaari, 2001.10705

Dipole-target scattering amplitude (IP-Sat)

$N(\mathbf{r}_T, \mathbf{b}_T, x) = 1 - \exp\left(-\mathbf{r}_T{}^2 F(\mathbf{r}_T, x) T_p(\mathbf{b}_T)\right)$ **accesses to the spatial structure ($T_{p/A}$)**

$F(\mathbf{r}_T, x) = \frac{\pi^2}{2N_c}\alpha_s(\mu^2) x g(x, \mu^2)$. $xg(x, \mu^2)$, gluon density at x and scale μ^2 $(\mu^2 \sim \mu_0^2 + 1/r_T^2)$.

$$\mathcal{A}^{\gamma^* p \to Vp} \sim \int \mathrm{d}^2 b \mathrm{d}z \mathrm{d}^2 r \Psi^{\gamma^*} \Psi^{V}(r, z, Q^2) \mathbf{e}^{-\mathbf{ib}\cdot\boldsymbol{\Delta}} N(r, x, b)$$

- Diffractive scattering amplitude is roughly proportional to Fourier transform of the spatial structure function of target (Tp/A).

Miettinen, Pumplin, PRD 18, 1978; Caldwell, Kowalski, 0909.1254; Mäntysaari, Schenke, 1603.04349; Mäntysaari, 2001.10705

Dipole-target scattering amplitude (CGC)

- The dipole amplitude N can be calculated from Wilson line V(x)

$$N\left(\mathbf{b}=\frac{\mathbf{x}+\mathbf{y}}{2},\mathbf{r}=\mathbf{x}-\mathbf{y},x_{\mathbb{P}}\right)=1-\frac{1}{N_c}\mathrm{Tr}\left(V(\mathbf{x})V^{\dagger}(\mathbf{y})\right).\quad V(\mathbf{x})=P\exp\left(-ig\int dx^{-}\frac{\rho(x^{-},\mathbf{x})}{\boldsymbol{\nabla}^2+m^2}\right)$$

- Using MV model for Gaussian distribution of color charge ρ:

$$\langle\rho^a(\mathbf{b}_\perp)\rho^b(\mathbf{x}_\perp)\rangle=g^2\mu^2(x,\mathbf{b}_\perp)\delta^{ab}\delta^{(2)}(\mathbf{b}_\perp-\mathbf{x}_\perp)$$

Q_s: saturation scale, $Q_s/g^2\mu$ is a free parameter, Q_s is determined from IP-Sat parametrization.

- Or, equivalently, factorize $\mu(x,\mathbf{b}_\perp)\sim T(\mathbf{b}_\perp)\mu(x)$

N(r, x, b) accesses to the spatial structure of the target ($T_{p/A}$).

Schenke , etc.al. PhysRevLett.108.252301 , PhysRevC.86.034908, Mäntysaari, Schenke, 1603.04349;

Coherent and incoherent processes

- **Coherent** $\sigma_{\text{coherent}} \sim |\langle \mathcal{A} \rangle_\Omega|^2$

Target stays intact, (<initial state| = |final state>)
Probes the average shape of the target.

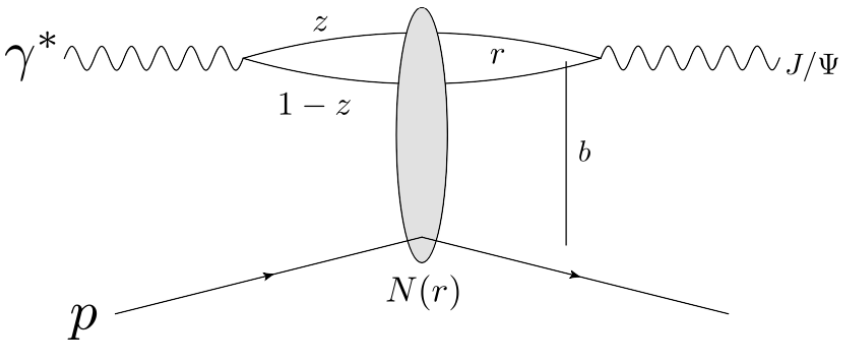

- **Incoherent** $\sigma_{\text{incoherent}} \sim \langle |\mathcal{A}|^2 \rangle_\Omega - |\langle \mathcal{A} \rangle_\Omega|^2$

Target breaks apart, (<initial state| ≠ |final state>)

Probes the variance of event-by-event initial state fluctuations in target structure.

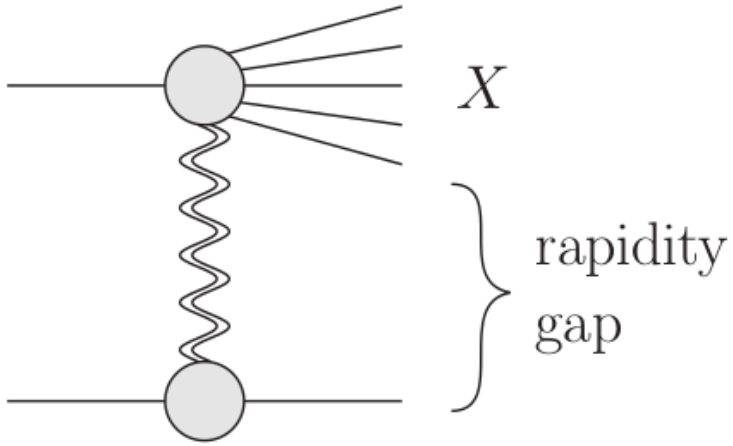

- Experimental signature: rapidity gap.
- Theoretically: no net color transfer.

Miettinen, Pumplin, PRD 18, 1978; Caldwell, Kowalski, 0909.1254; Mäntysaari, Schenke, 1603.04349; Mäntysaari, 2001.10705

Proton geometry fluctuations

- Proton's event-by-event fluctuating density profile:

$$T_p(\mathbf{b}_\perp) = \frac{1}{N_q}\sum_{i=1}^{N_q} p_i T_q(\mathbf{b}_\perp - \mathbf{b}_{\perp,i}), \quad P(\ln p_i) = \frac{1}{\sqrt{2\pi}\sigma}\exp\left[-\frac{\ln^2 p_i}{2\sigma^2}\right].$$

- The density profile of each spot is:

$$T_q(\vec{b}) = \frac{1}{2\pi B_q} e^{-b^2/(2B_q)}$$

- The spot positions $\vec{b_i}$ are sampled from:

$$P(b_i) = \frac{1}{2\pi B_{qc}} e^{-b_i^2/(2B_{qc})}$$

Schenke , etc.al. PhysRevLett.108.252301 , PhysRevC.86.034908, Mäntysaari, Schenke, 1603.04349;

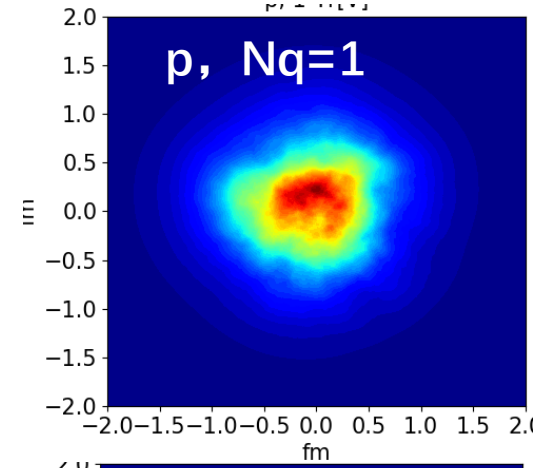

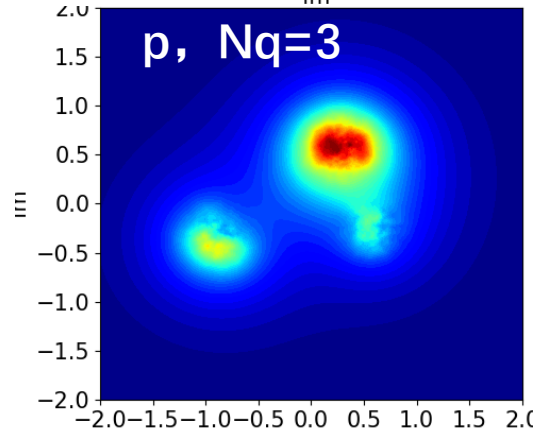

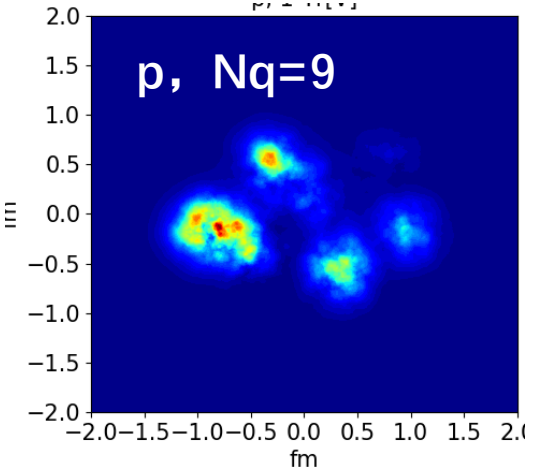

Model parameters and the Exp. Data (γ^* + p → J/ψ + p*)

Parameterize proton shape (T_p)

- Number of hot spots N_q
- Proton size B_{qc}
- Hot spot size B_q
- Hot spot density fluctuations σ
- Min. distance between hot spots $d_{q,min}$
- Overall color charge density: $Qs(x)/g^2\mu$
- Infrared regulator m

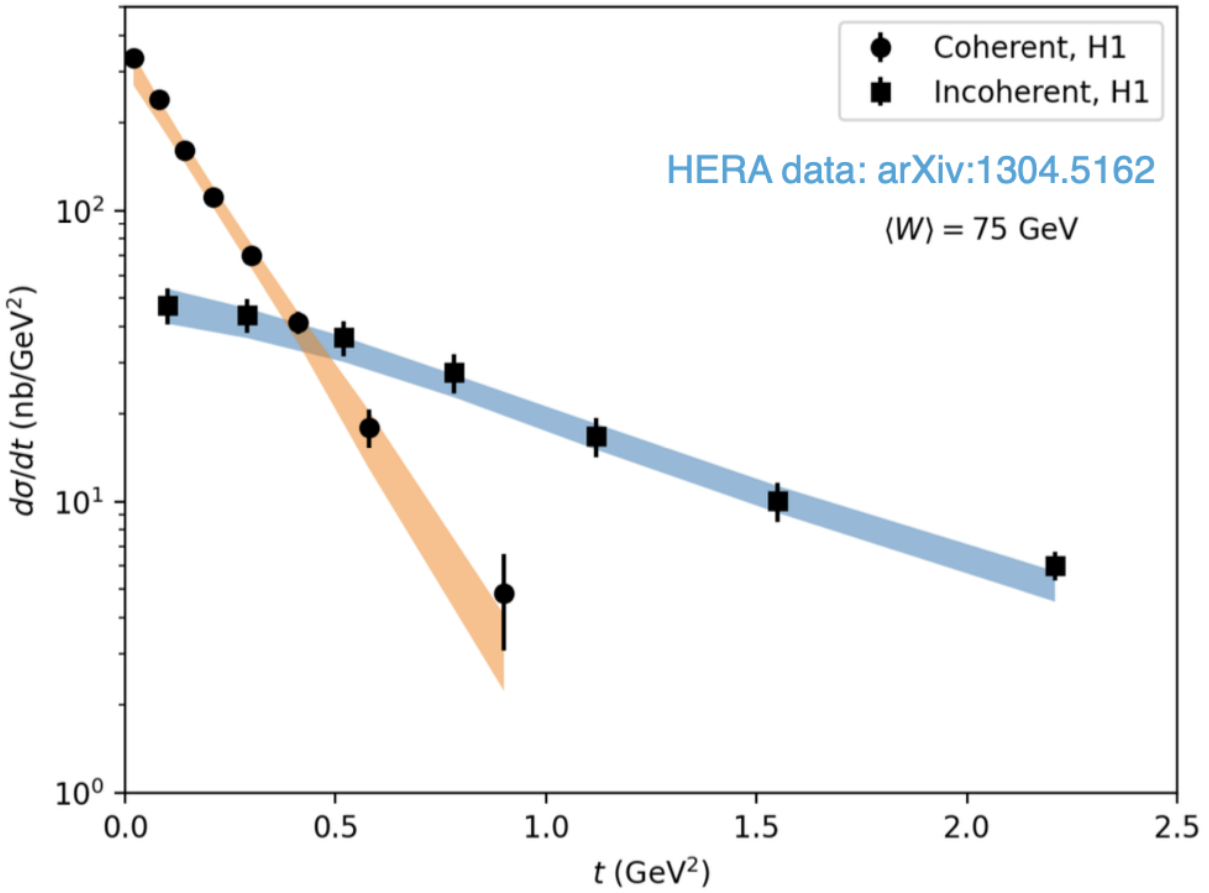

- 7D parameter space; generated 1000 training points for the model emulator

H.Mantysaari, B.Schenke, C. Shen and W. Zhao, Phys. Lett. B 833 (2022), 137348.

Bayes Theorem

Thomas Bayes

Probabilistic constraints on parameters

Mean value of **measurements**

Experimental and theoretical **uncertainties**

$$\mathbf{posterior}(p|D) \propto \boldsymbol{prior}(p) \times \boldsymbol{exp}\left(-\frac{1}{2}\left(D - \boldsymbol{Model}(p)\right)^{T} \boldsymbol{Cov}^{-1}\left(D - \boldsymbol{Model}(p)\right)\right)$$

External constraints on parameters: positivity or range of allowed values, "probabilistic theoretical constraints", …

Prediction of model for given set of parameters

Ref: Jean-Francois, APS, 2021

- Constrain the model parameters by the Bayesian analysis.

Closure tests

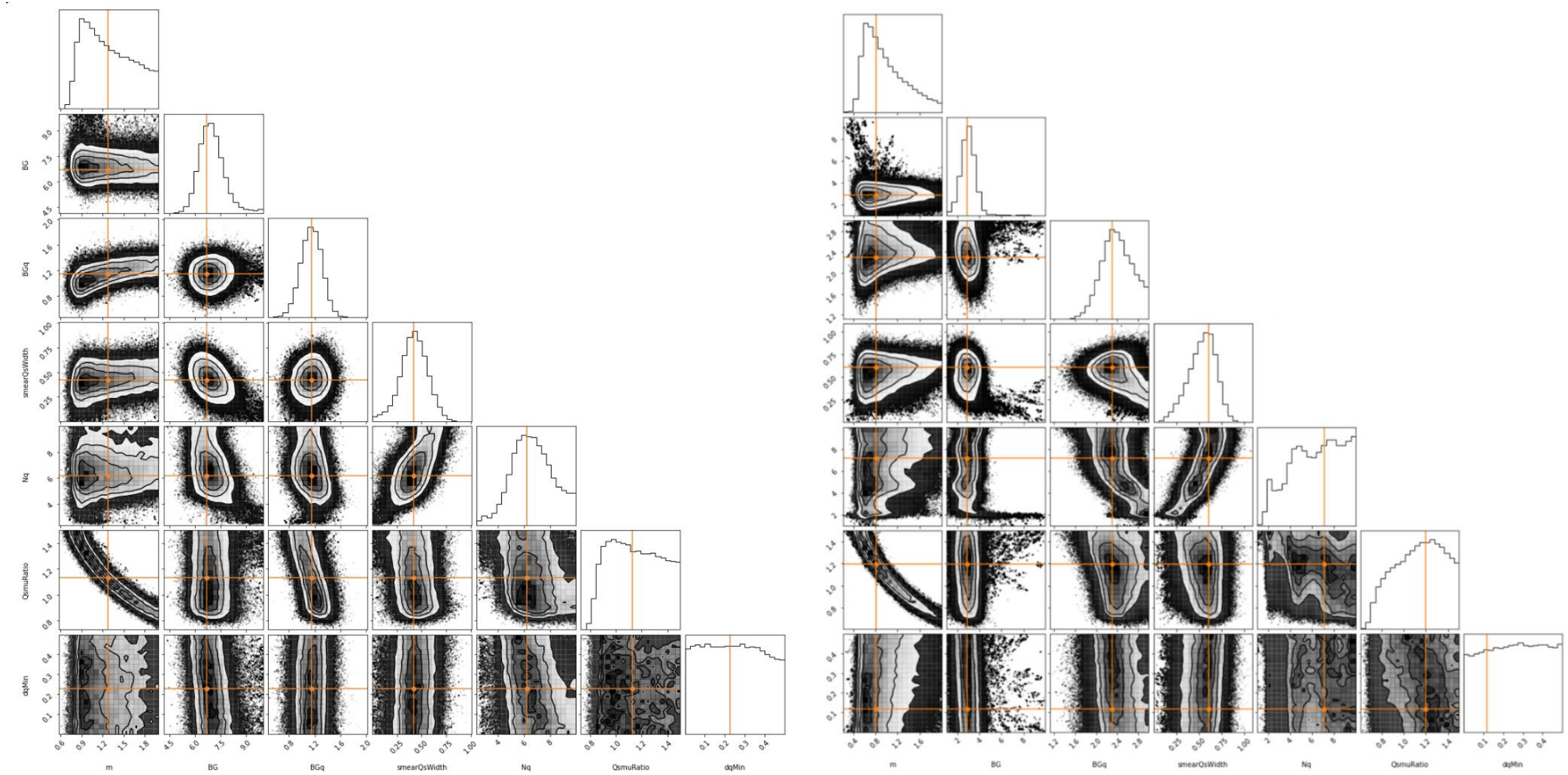

H.Mantysaari, B.Schenke, C. Shen and W. Zhao, Phys. Lett. B 833 (2022), 137348.

Building intuition for the model parameters

- Proton size:

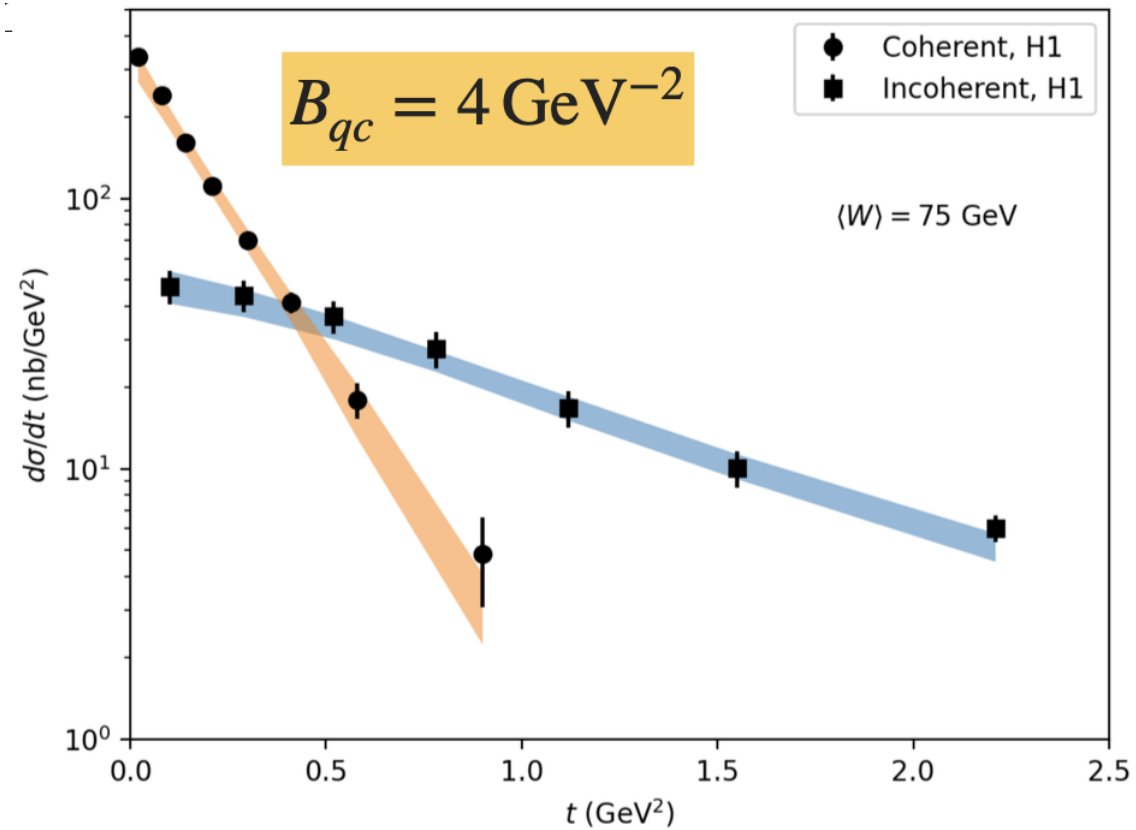

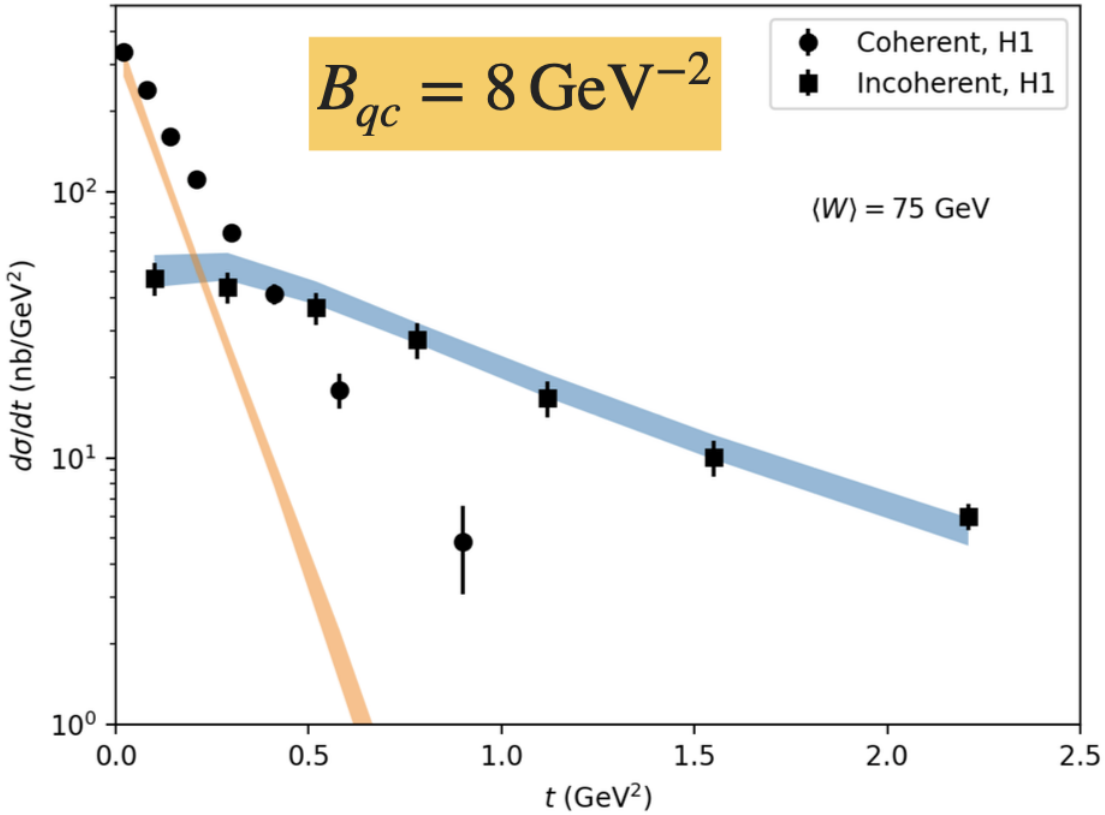

- The proton size mainly affects the coherent cross section.

H.Mantysaari, B.Schenke, C. Shen and W. Zhao, Phys. Lett. B 833 (2022), 137348.

Building intuition for the model parameters

- Hot spot size:

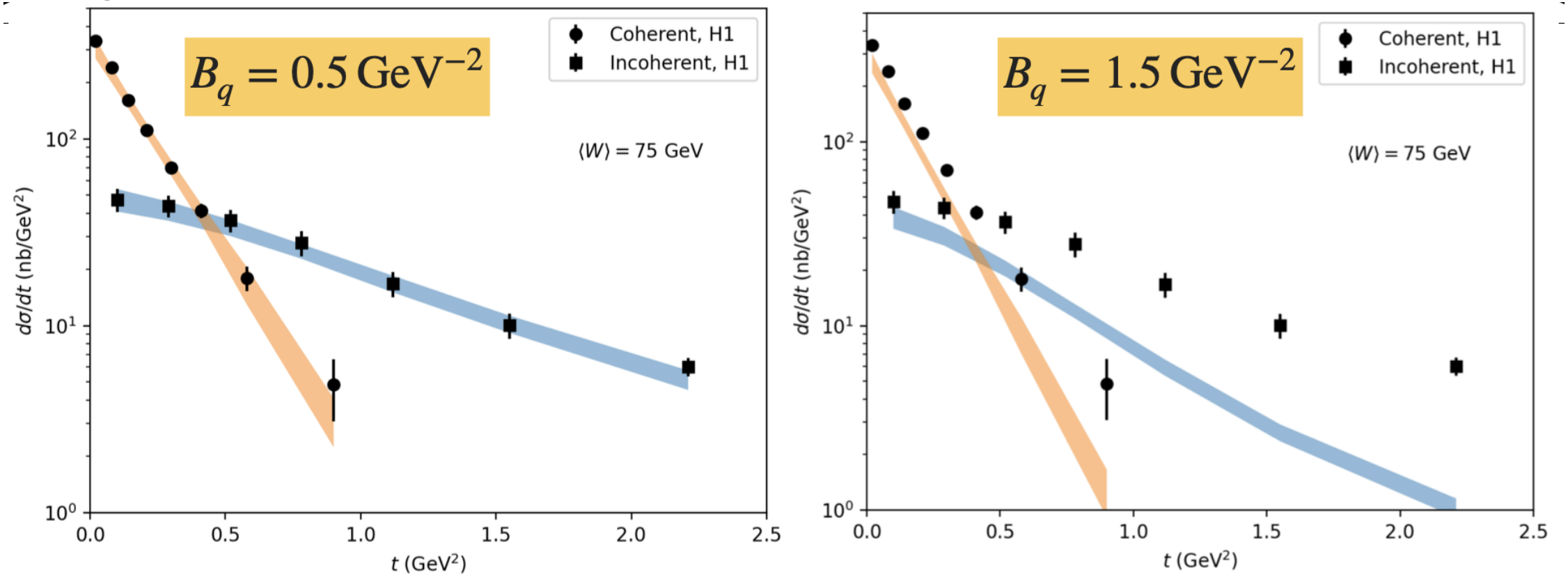

- The shape of incoherent cross-section is sensitive to the sub-nucleonic hot spot size

H.Mantysaari, B.Schenke, C. Shen and W. Zhao, Phys. Lett. B 833 (2022), 137348.

Building intuition for the model parameters

- Infrared regulator:

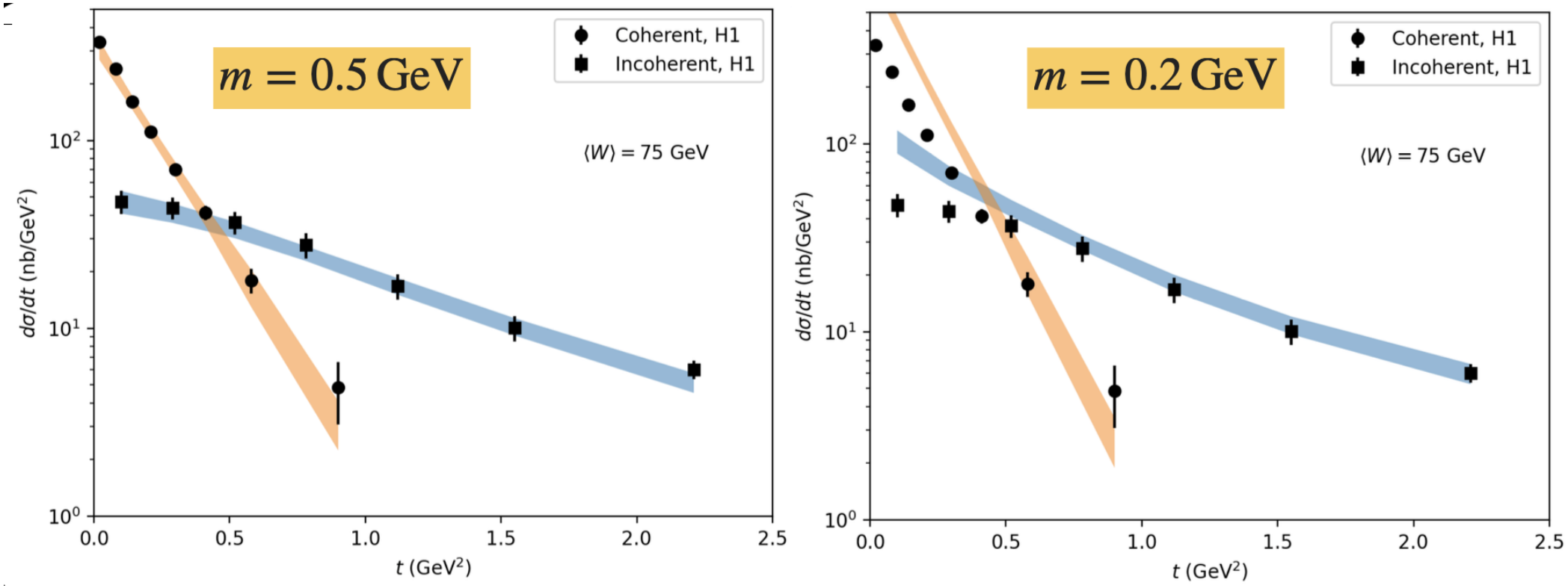

- A small infrared regulator extends density tail in the large scale region, which results in increase of coherent and incoherent cross-section at low |t|.

H.Mantysaari, B.Schenke, C. Shen and W. Zhao, Phys. Lett. B 833 (2022), 137348.

Building intuition for the model parameters

- Overall color charge density:

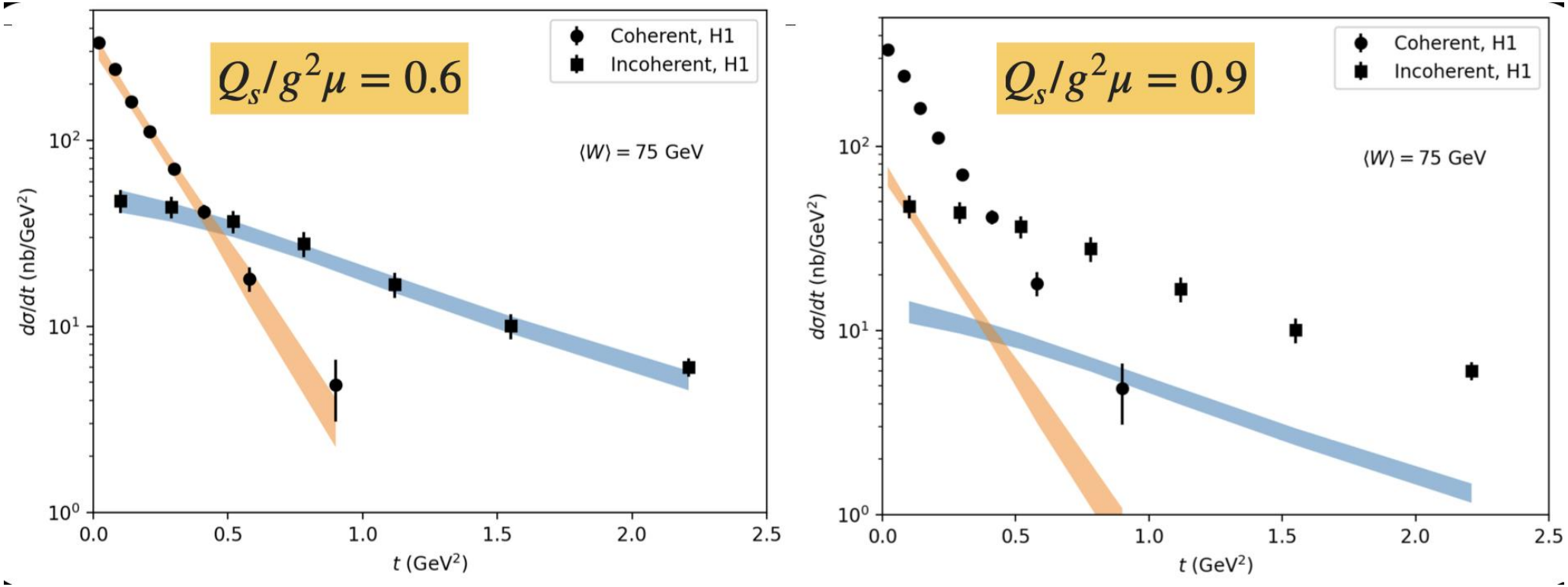

- A large $Q_s/g^2\mu$ ratio gives small color charge density, which reduces the magnitudes of both coherent and incoherent cross-sections.

H.Mantysaari, B.Schenke, C. Shen and W. Zhao, Phys. Lett. B 833 (2022), 137348.

Building intuition for the model parameters

- Hot spot density fluctuations:

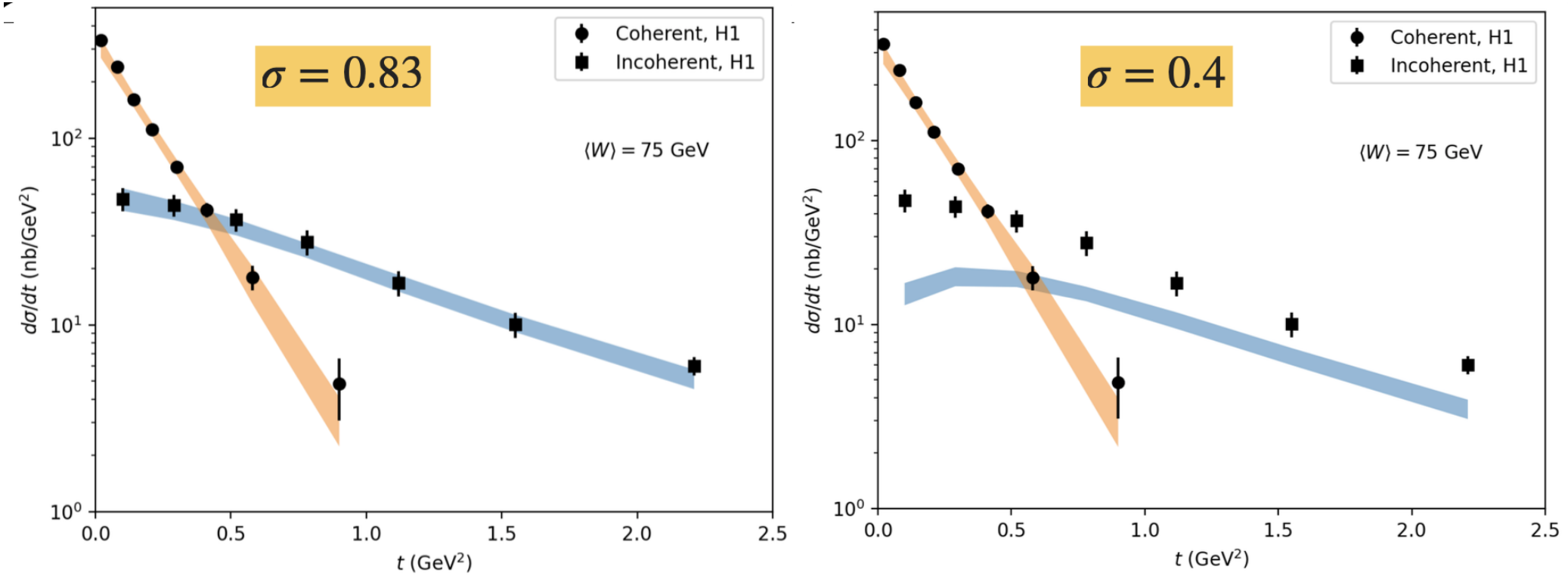

- A small variance of the density fluctuations reduces the magnitude of incoherent cross-section

H.Mantysaari, B.Schenke, C. Shen and W. Zhao, Phys. Lett. B 833 (2022), 137348.

Building intuition for the model parameters

- Number of hot spots:

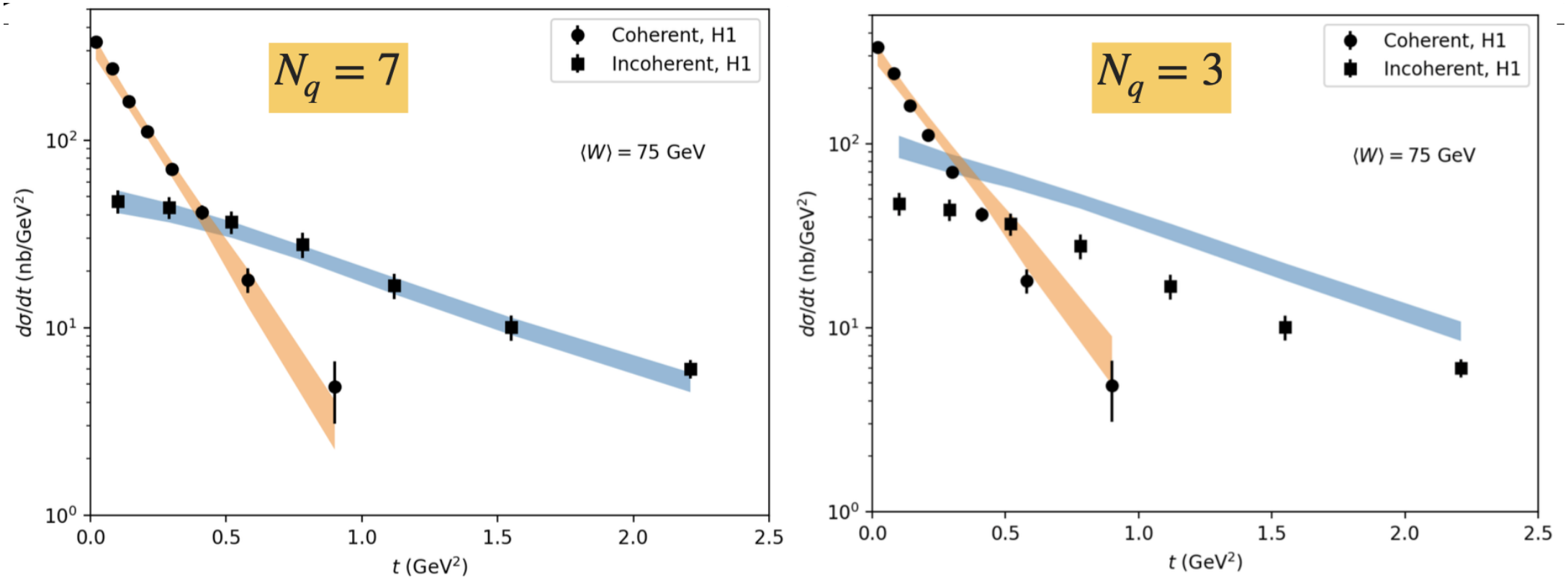

- Small number of hot spots increases fluctuations, which results in large incoherent cross-sections

H.Mantysaari, B.Schenke, C. Shen and W. Zhao, Phys. Lett. B 833 (2022), 137348.

Building intuition for the model parameters

- Minimum distance between hot spots

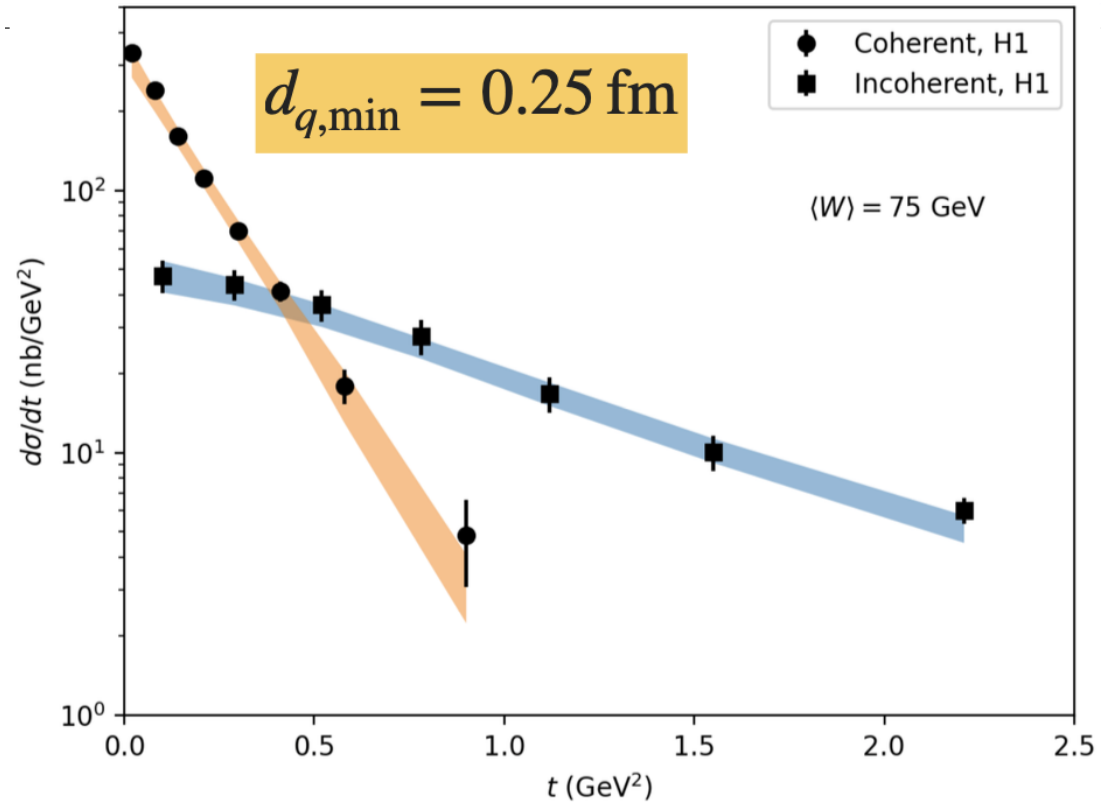

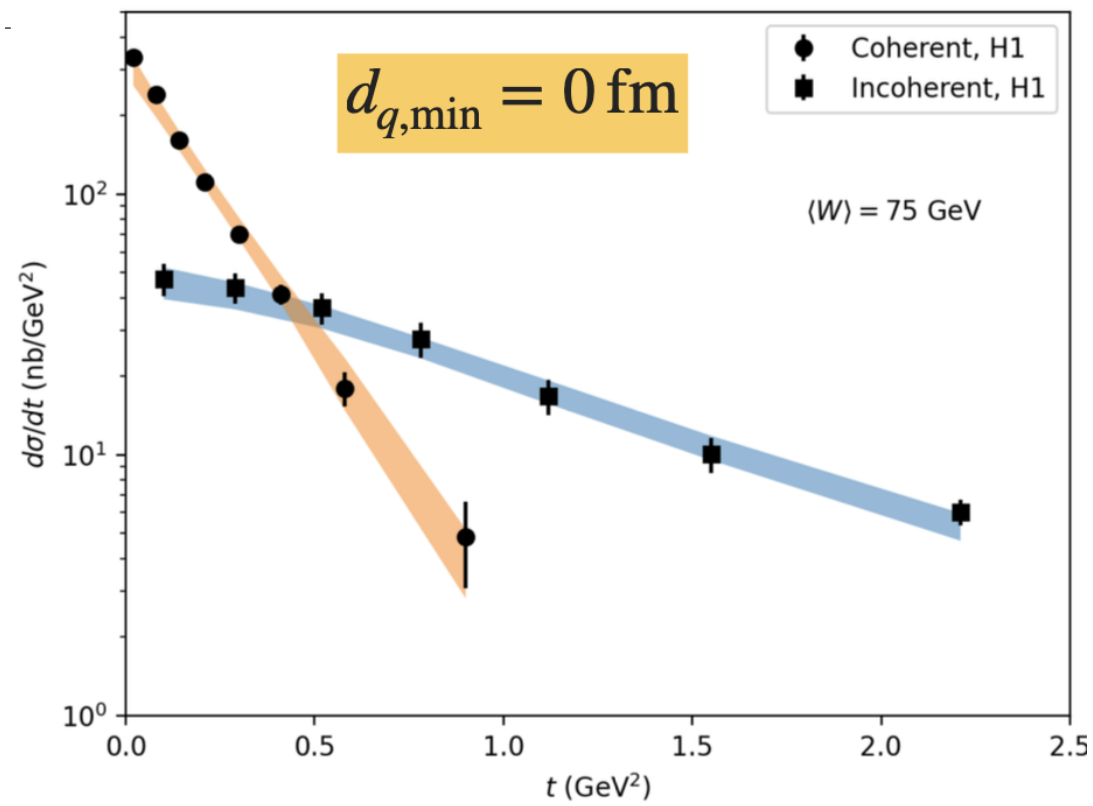

- No clear sensitivity on the intra distance between hot spots.

H.Mantysaari, B.Schenke, C. Shen and W. Zhao, Phys. Lett. B 833 (2022), 137348.

Building intuition for the model parameters

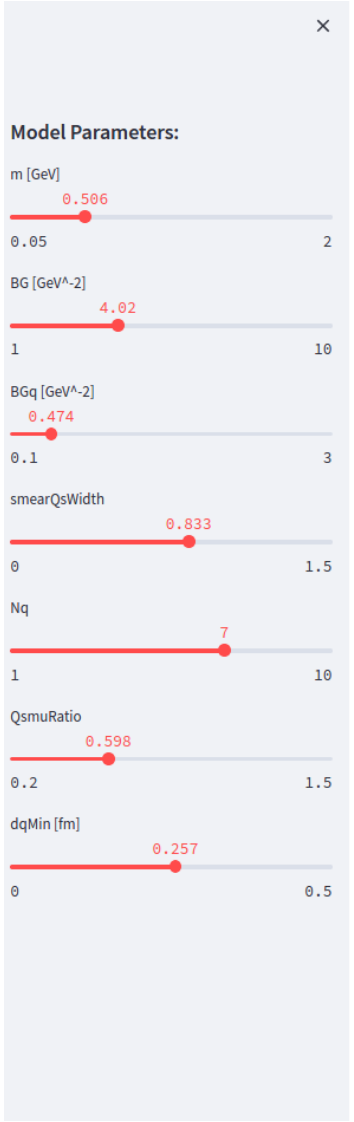

IPGlasma + Diffraction

This is an interactive web page that emulates the J/ψ photoproduction cross sections in deep inelastic scatterings of protons using the IPGlasma model.

This work is based on arXiv:2202.01998 [hep-ph]

One can adjust the model parameters on the left sidebar.

The colored bands in the figure show the emulator estimations with their uncertainties. The compared experimental data are from the H1 Collaboration, Eur. Phys. J. C 73 (2013) No. 6, 2466

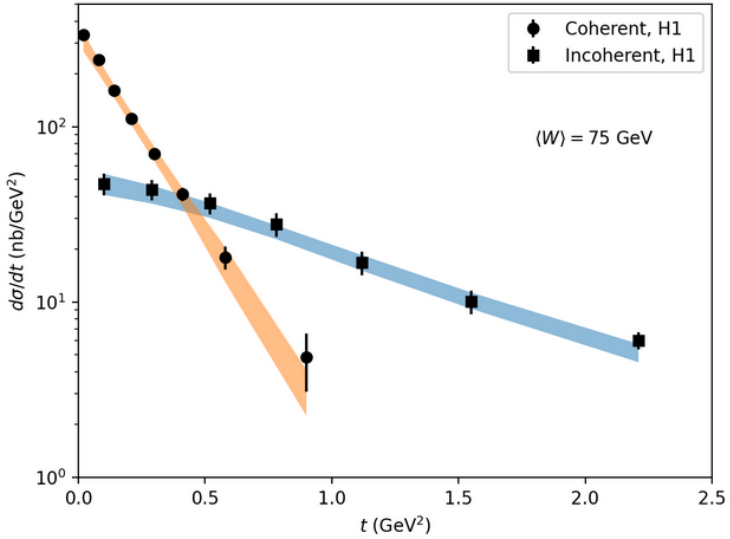

Posterior Samples:

Download CSV (variable Nq)

Play it by yourself: https://chunshen1987-ipglasmadiffraction-ipglasmadiffraction-app-hw6l4b.streamlit.app

H.Mantysaari, B.Schenke, C. Shen and W. Zhao, Phys. Lett. B 833 (2022), 137348.

Posterior Distribution

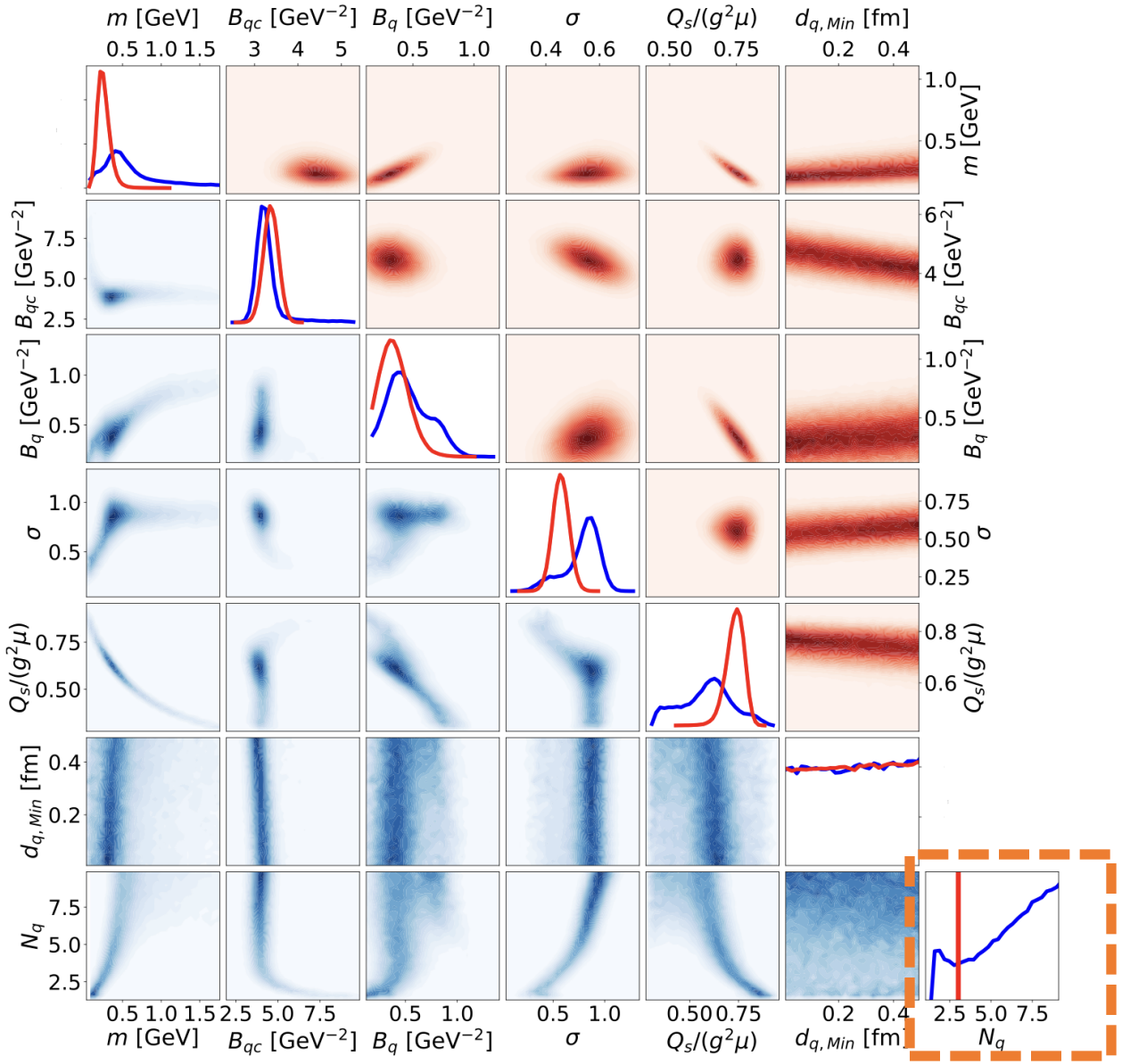

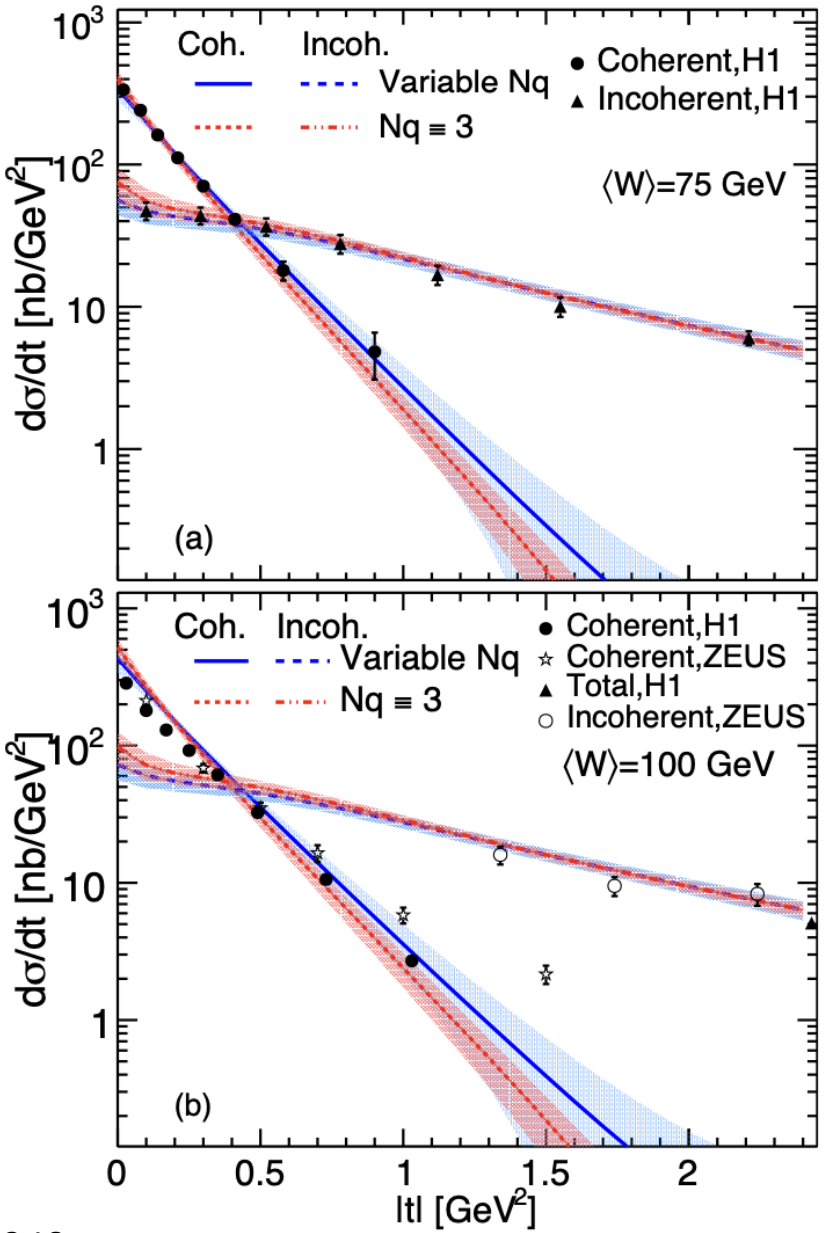

H.Mantysaari, B.Schenke, C. Shen and W. Zhao, Phys. Lett. B 833 (2022), 137348.

Proton & hotspot sizes at high energy

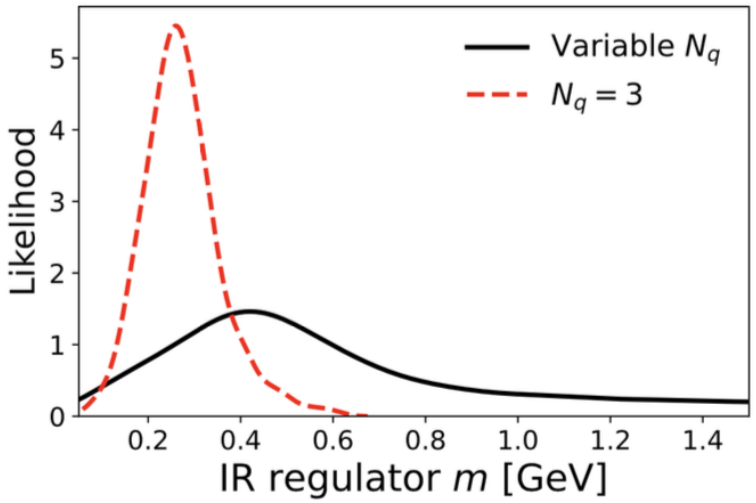

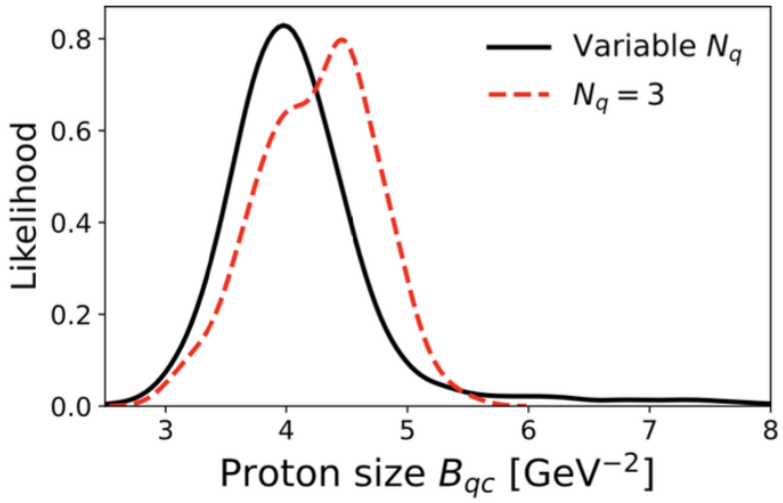

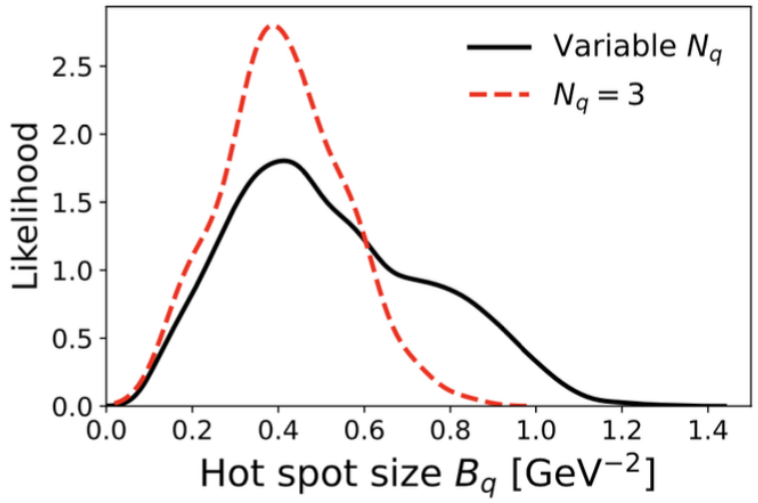

- Some parameters are well constrained .
- Wider posterior distributions for the varying Nq case.
- The 2D RMS proton radius $R_{rms} = \sqrt{2(B_{qc} + B_q)} \sim 0.6$ fm, which is consistent with the results in heavy-ion collisions.

H.Mantysaari, B.Schenke, C. Shen and W. Zhao, Phys. Lett. B 833 (2022), 137348.
H.Mantysaari, B.Schenke, C. Shen and W. Zhao, [arXiv:2208.00396 [hep-ph]].
G. Giacalone, B. Schenke and C. Shen, Phys. Rev. Lett. 128, 042301 (2022)

Degeneracy in the number of hot spots

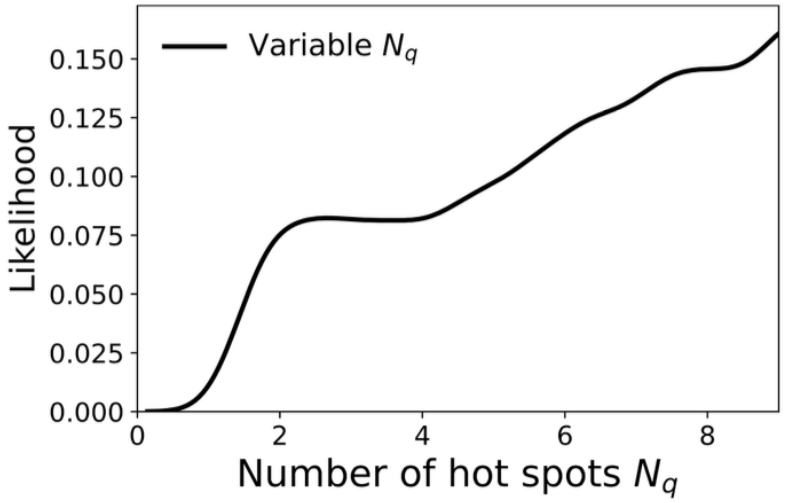

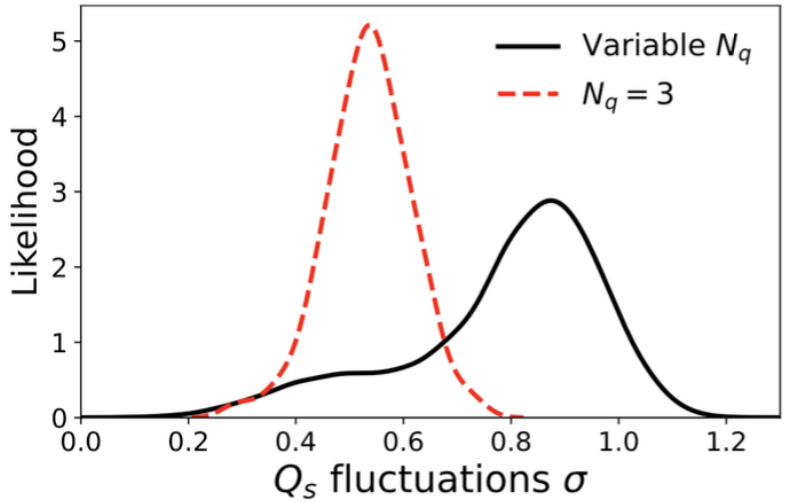

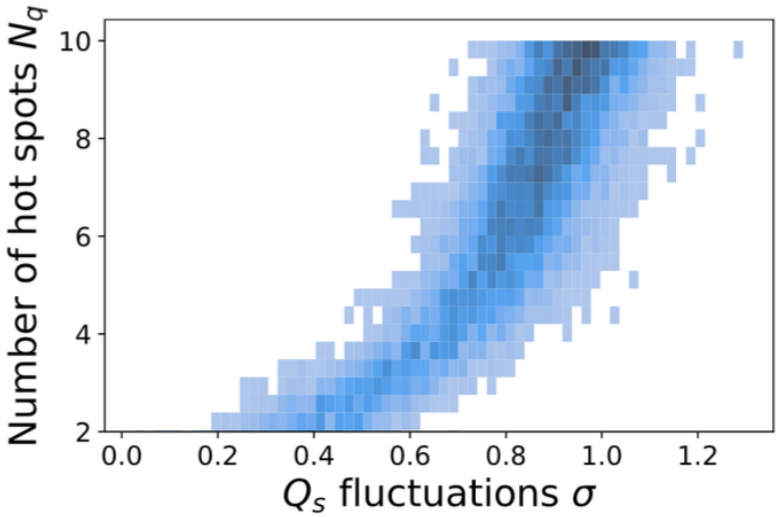

- The likelihood of number of hot spots Nq increases monotonously.
- Large Nq partially compensated by large Qs fluctuations, $\sigma \propto \sqrt{N_q}$, "number of effective hot spots" < Nq
- **Proton's event-by-event fluctuating density profile:**

$$T_p(\mathbf{b}_\perp) = \frac{1}{N_q}\sum_{i=1}^{N_q} p_i T_q(\mathbf{b}_\perp - \mathbf{b}_{\perp,i}), \quad P(\ln p_i) = \frac{1}{\sqrt{2\pi}\sigma}\exp\left[-\frac{\ln^2 p_i}{2\sigma^2}\right].$$

H. Mantysaari, B.Schenke, C. Shen and W. Zhao, Phys. Lett. B 833 (2022), 137348.
H. Mantysaari, B.Schenke, C. Shen and W. Zhao, [arXiv:2208.00396 [hep-ph]].

MAP of fixed Nq=3 and Nq=9

Parameter	Description	$N_q = 9$	$N_q = 3$
m [GeV]	Infrared regulator	0.780	0.246
B_{qc} [GeV^{-2}]	Proton size	3.98	4.45
B_q [GeV^{-2}]	Hot spot size	0.594	0.346
σ	Magnitude of Q_s fluctuations	0.932	0.563
$Q_s/(g^2\mu)$	$Q_s \Rightarrow$ color charge density	0.492	0.747
$d_{q,\mathrm{Min}}$ [fm]	Min hot spot distance	0.265	0.254
N_q	Number of hot spots	3	9
S	Hydro normalization	0.1135	0.235

- The Nq=3 and Nq=9 have the different configurations at large length scales.
- “See” them by the different probes.

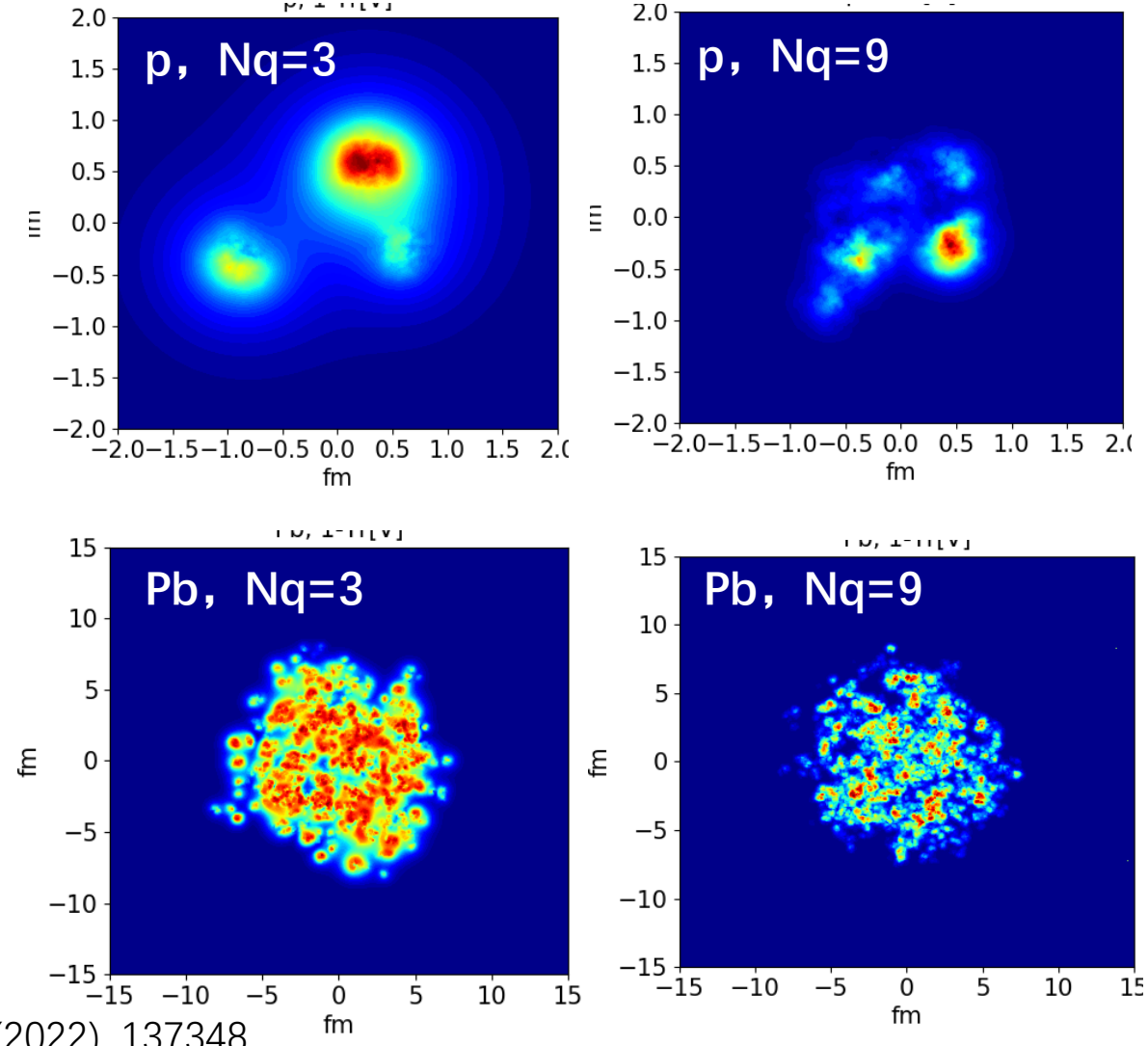

H. Mantysaari, B.Schenke, C. Shen and W. Zhao, Phys. Lett. B 833 (2022), 137348.
H. Mantysaari, B.Schenke, C. Shen and W. Zhao, [arXiv:2208.00396 [hep-ph]].

Probing protons at different resolutions

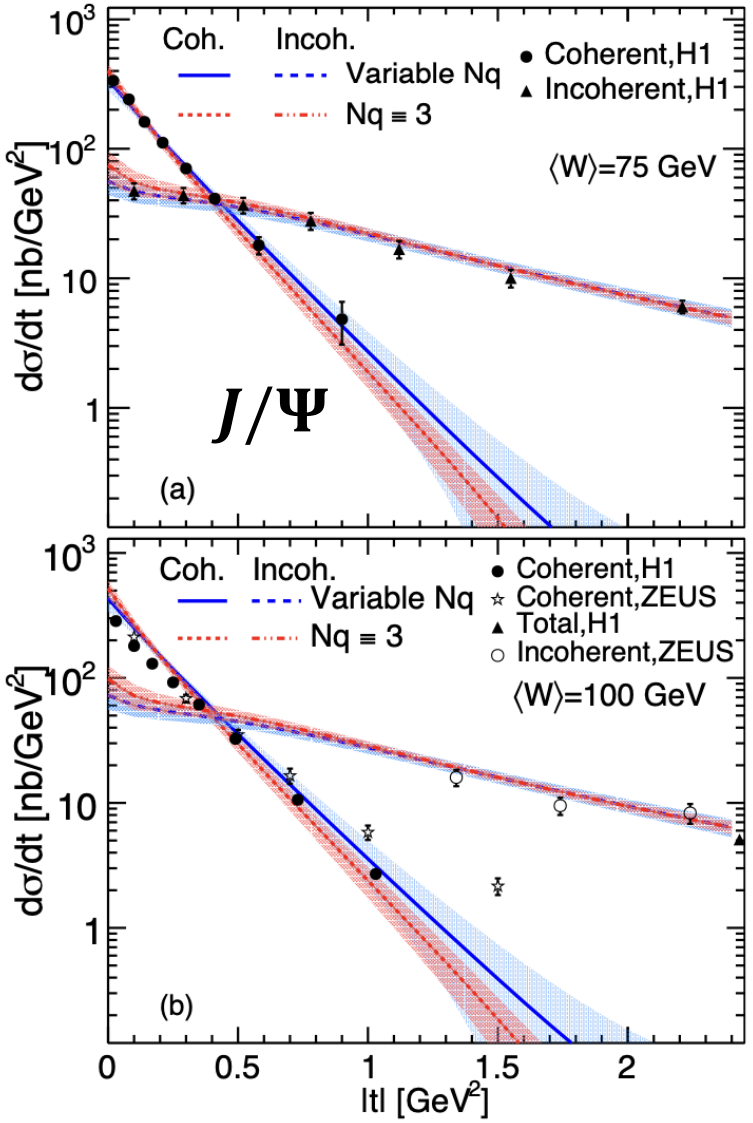

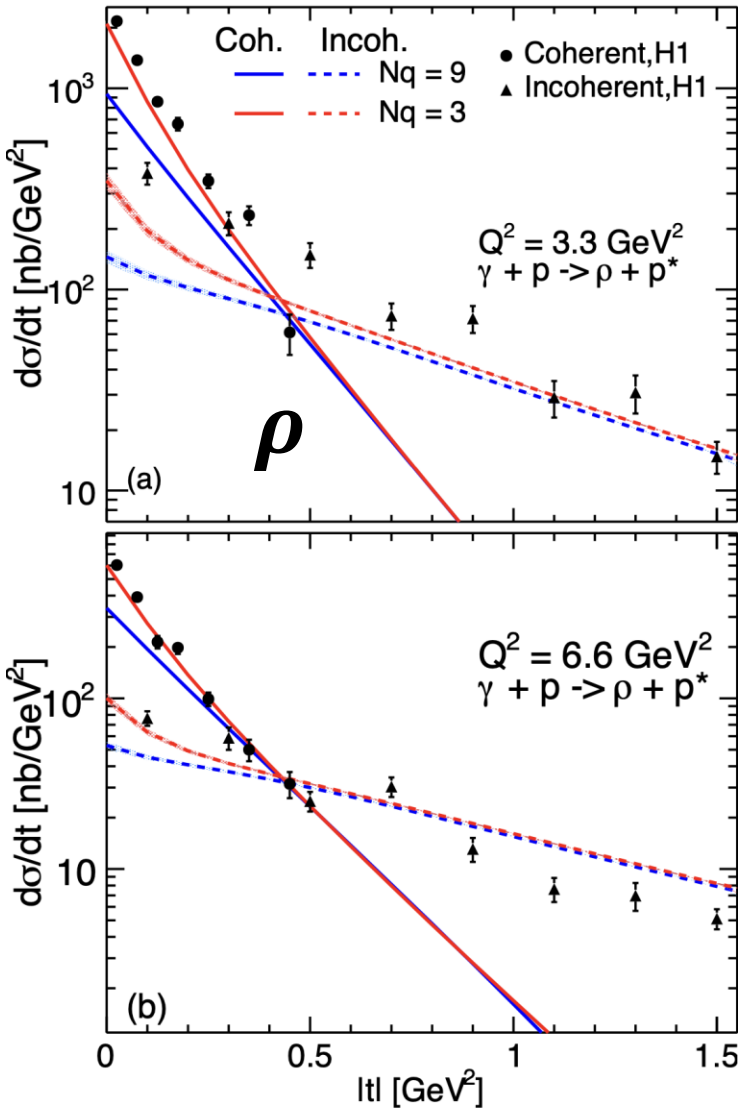

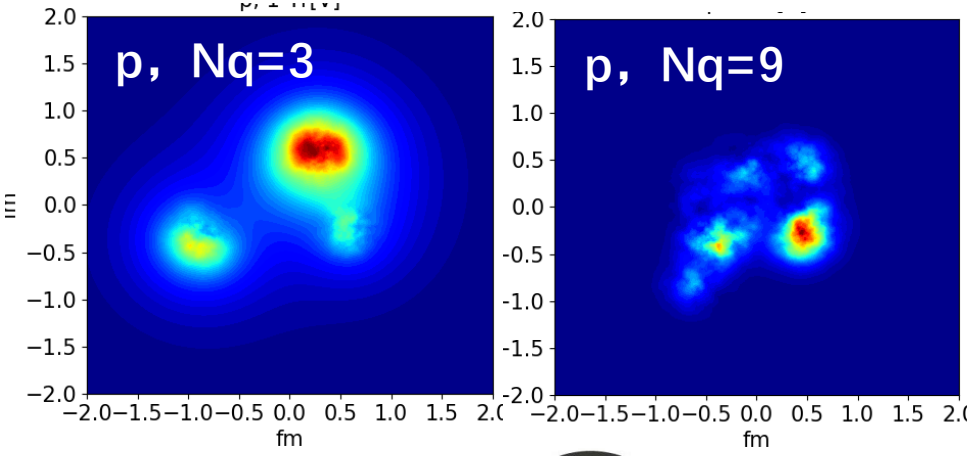

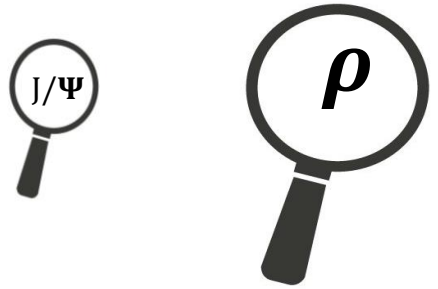

- The ρ mesons probe proton fluctuations at large length scales.
- Large differences observed for ρ productions between Nq=3 and Nq=9 MAPs.
- Larger Q^2, smaller difference.

H. Mantysaari, B.Schenke, C. Shen and W. Zhao, Phys. Lett. B 833 (2022), 137348, and in progress.

Connecting to Relativistic Nuclear Collisions

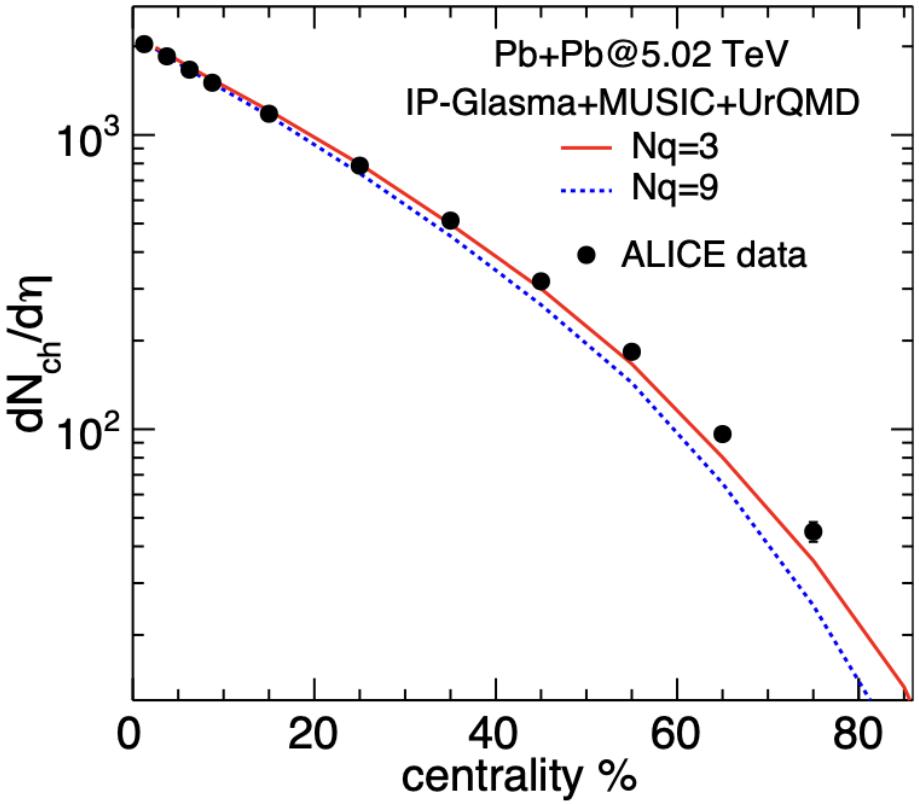

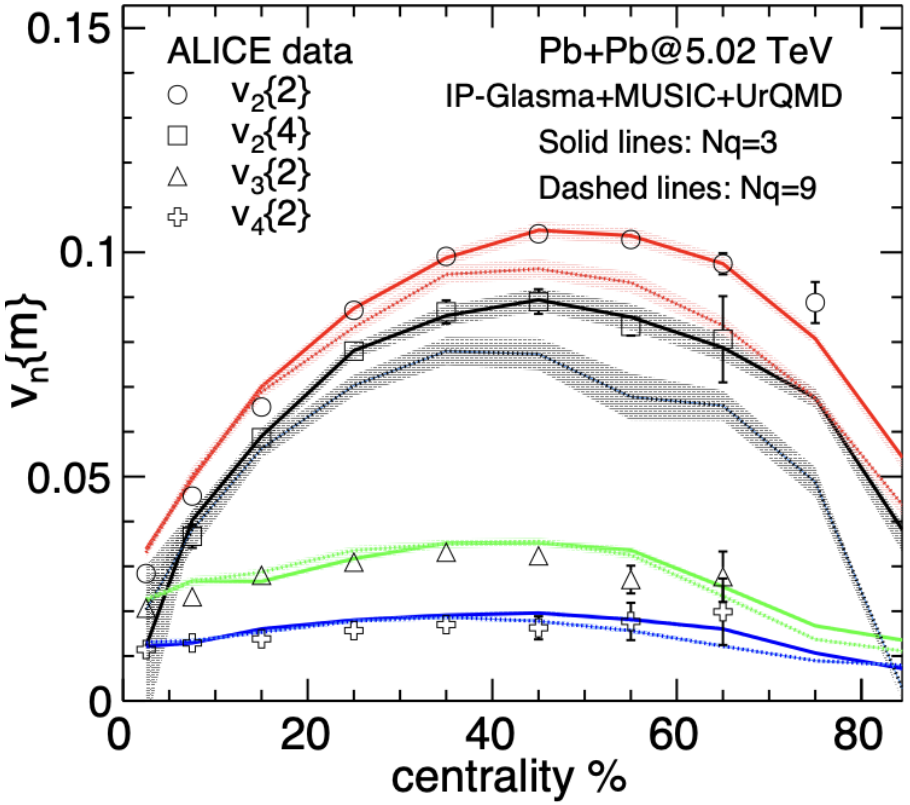

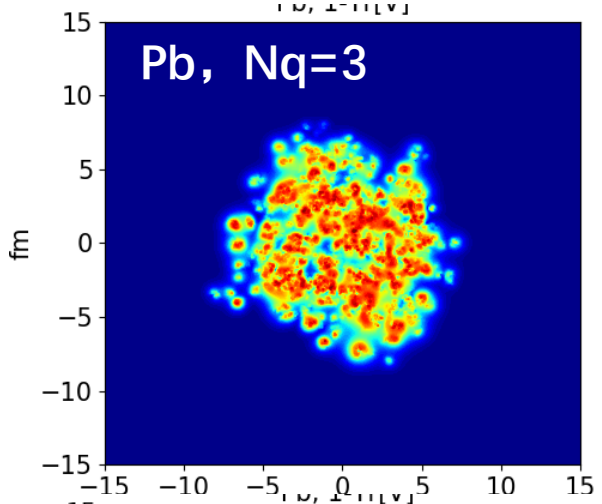

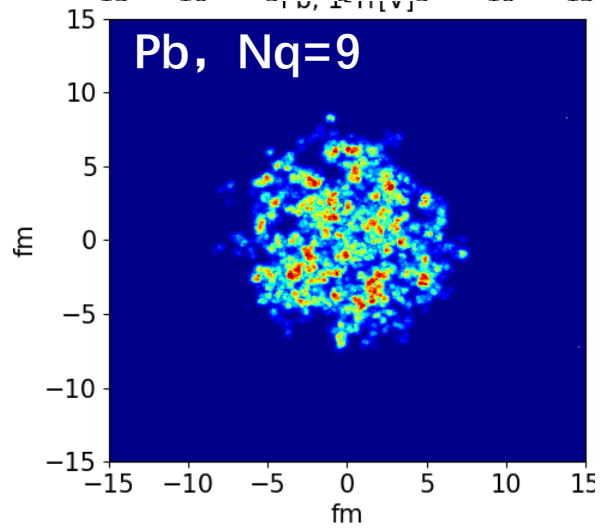

- The multiplicity distributions and elliptic flow coefficients in Pb+Pb collisions favor the small Nq case.

H.Mantysaari, B.Schenke, C. Shen and W. Zhao, Phys. Lett. B 833 (2022), 137348.
H.Mantysaari, B.Schenke, C. Shen and W. Zhao, [arXiv:2208.00396 [hep-ph]].

p + Pb Collisions

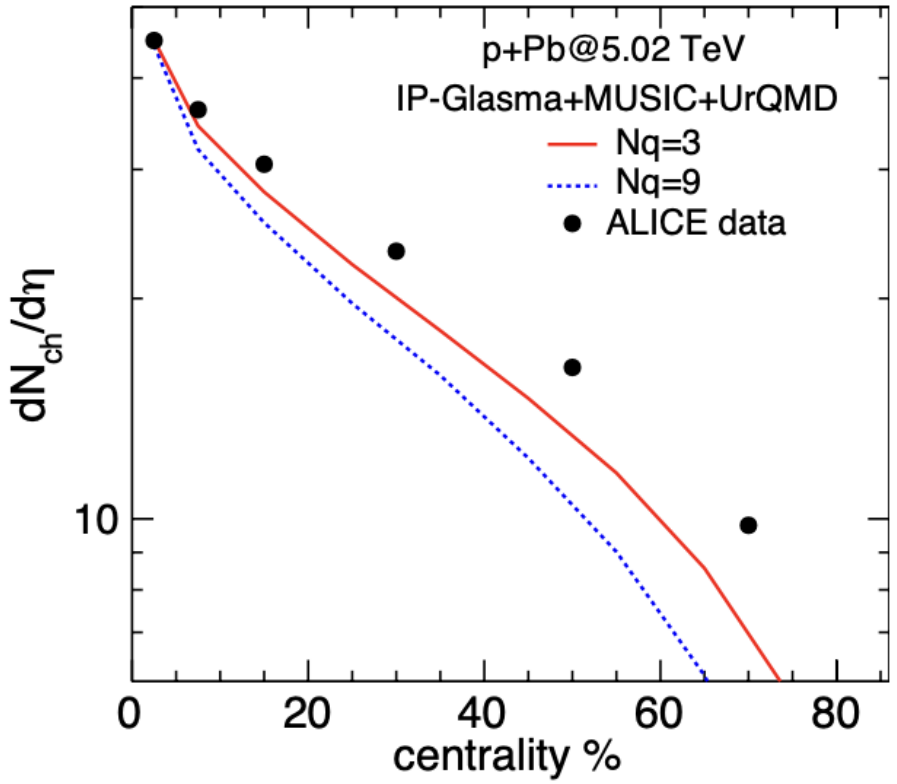

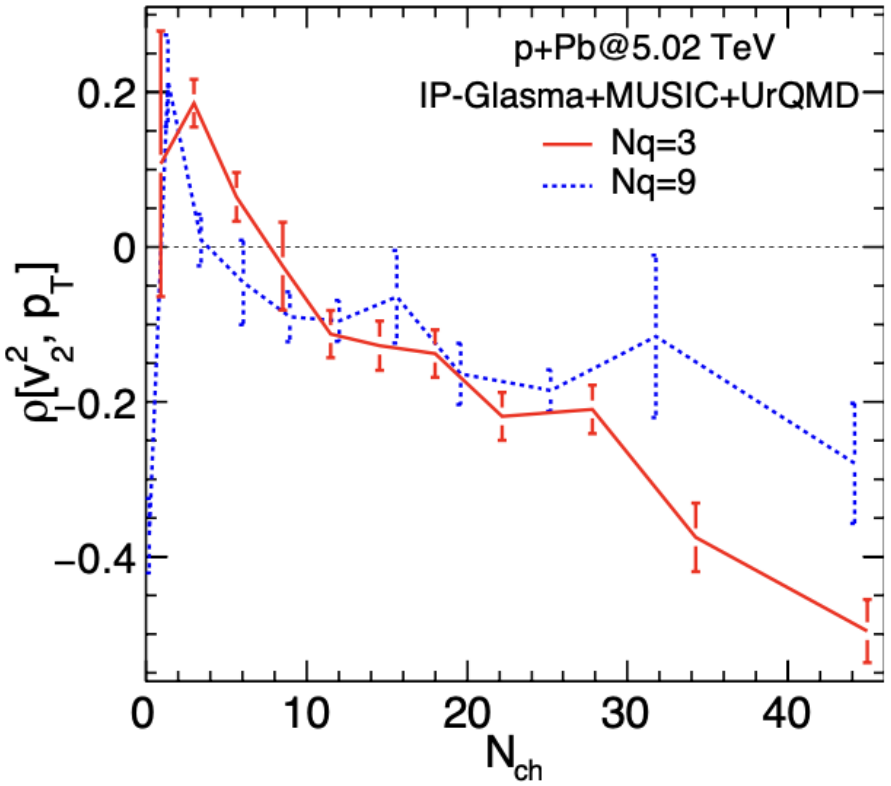

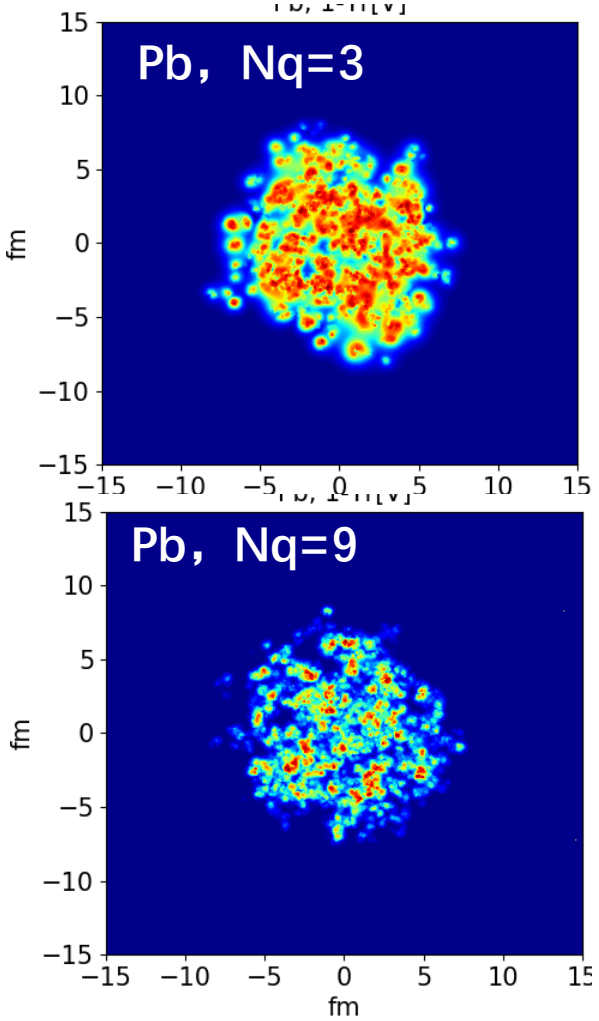

- Similar to Pb+Pb case, p+Pb favors the small Nq case as well.
- $v_2 - p_T$ correlator in p+Pb identified as a promising observable.
- We would like to explore more experimental constraints using HERA + LHC Pb+Pb and p+Pb data

H.Mantysaari, B.Schenke, C. Shen and W. Zhao, Phys. Lett. B 833 (2022), 137348.
H.Mantysaari, B.Schenke, C. Shen and W. Zhao, [arXiv:2208.00396 [hep-ph]].

Fixed Nq ≡ 1 cases

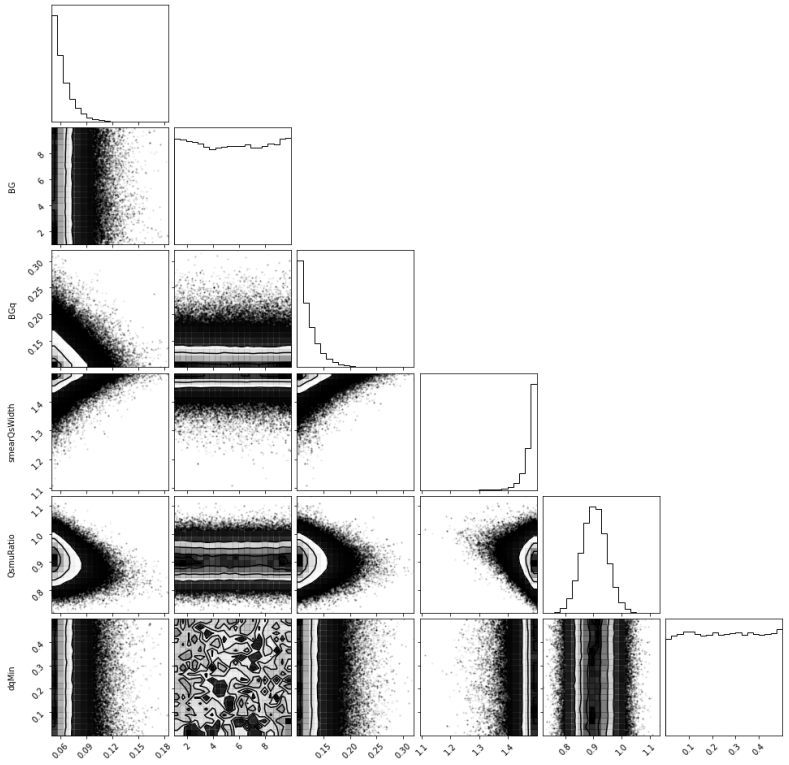

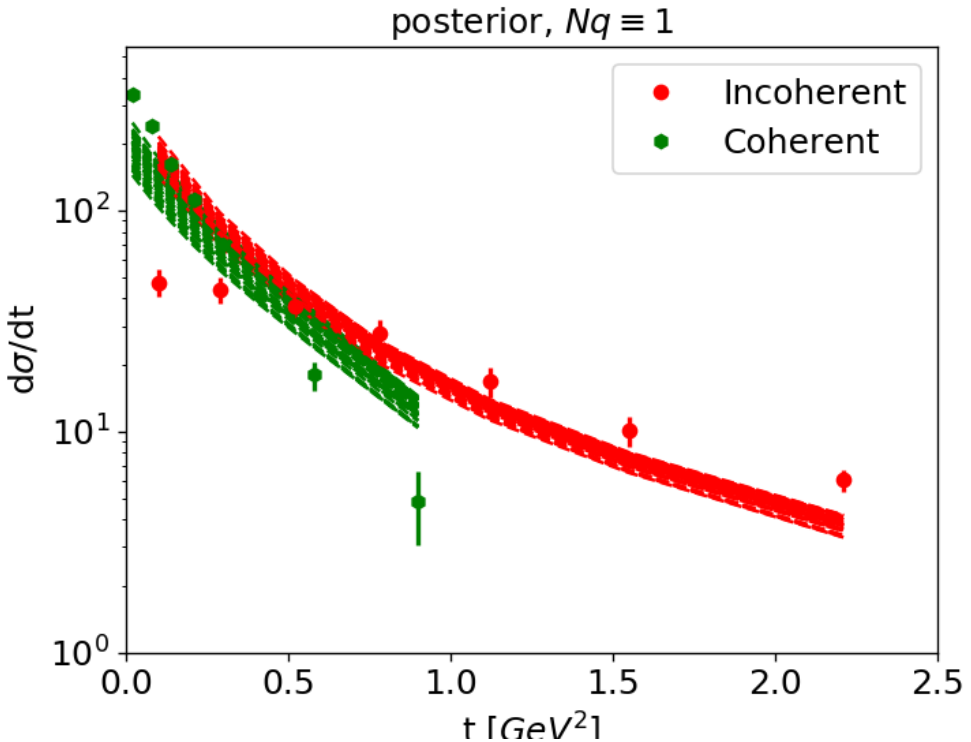

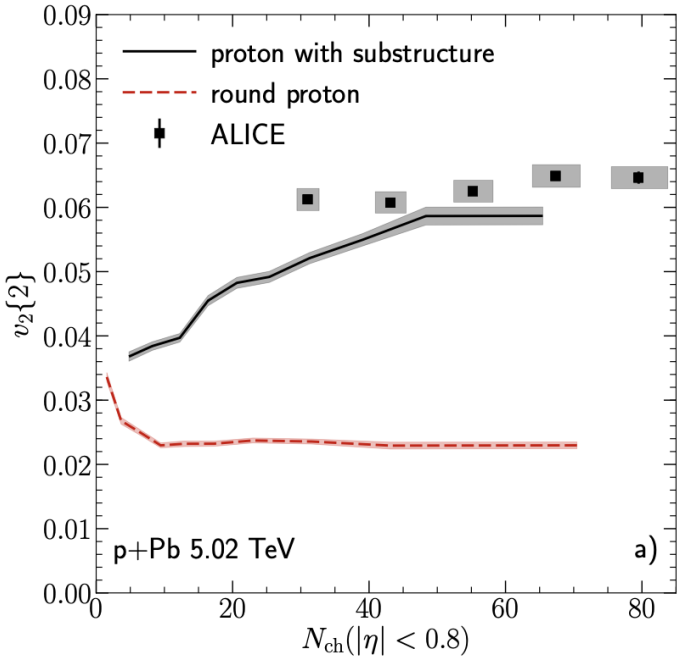

B. Schenke, Rept. Prog. Phys. 84, 082301 (2021).

- Bayesian analysis with fixed Nq≡1 can't extract the parameter set to fit the HERA data.
- It's consistent with the hydrodynamic results.

H.Mantysaari, B.Schenke, C. Shen and W. Zhao, Phys. Lett. B 833 (2022), 137348.

Accessing nuclear deformation at small x

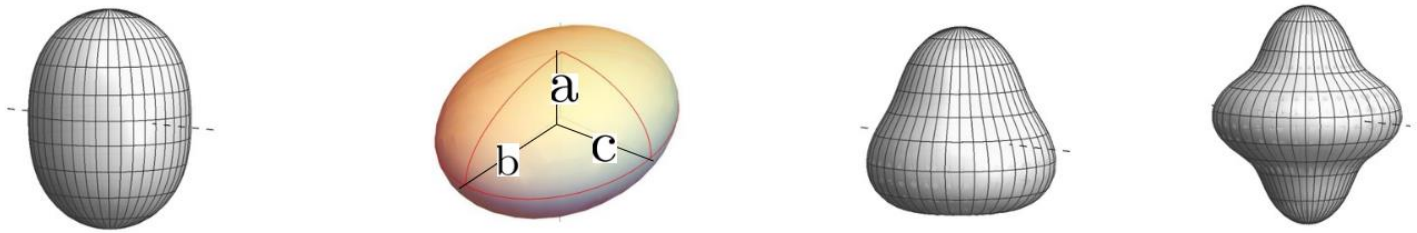

Nuclear structure

Generalized Woods-Saxon profile

$$\rho(r,\Theta,\Phi) \propto \frac{1}{1+\exp\left(\left[r-R(\Theta,\Phi)\right]/a\right)} \quad , \quad R(\Theta,\Phi) = R_0\left[1+\beta_2\left(\cos\gamma Y_{20}(\Theta)+\sin\gamma Y_{22}(\Theta,\Phi)\right)+\beta_3 Y_{30}(\Theta)+\beta_4 Y_{40}(\Theta)\right]$$

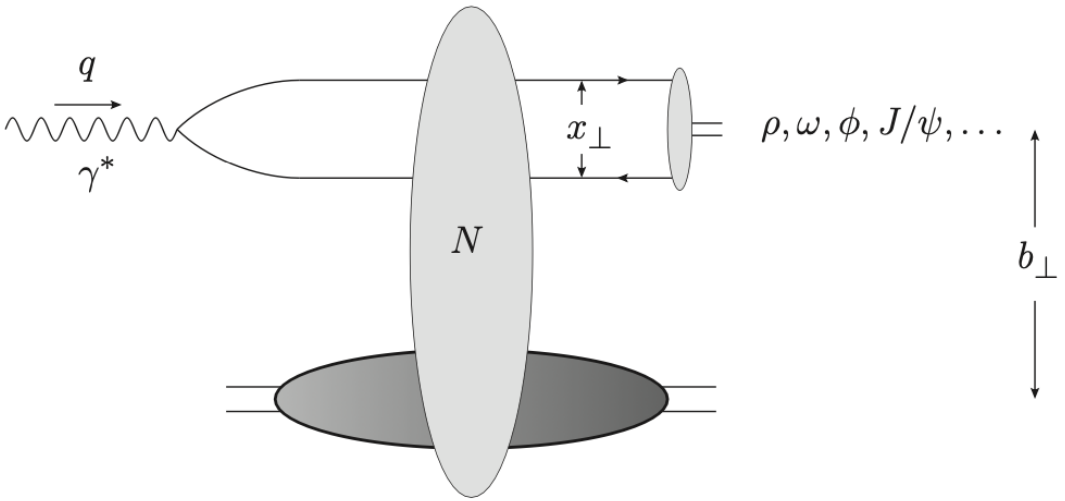

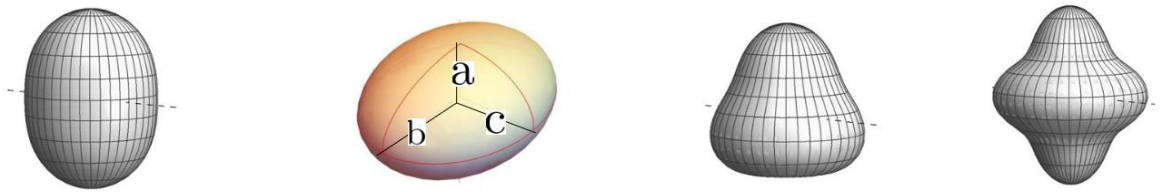

Taken from Giuliano's slide

- Sample nucleon positions based on the Wood—Saxon distribution.
- Different deformation parameters controls the geometric deformation at different length scale.
- Probe the nuclear geometric deformation (deformed gluon density distributions) by the diffractive process.

γ^* + U → J/ψ + U*

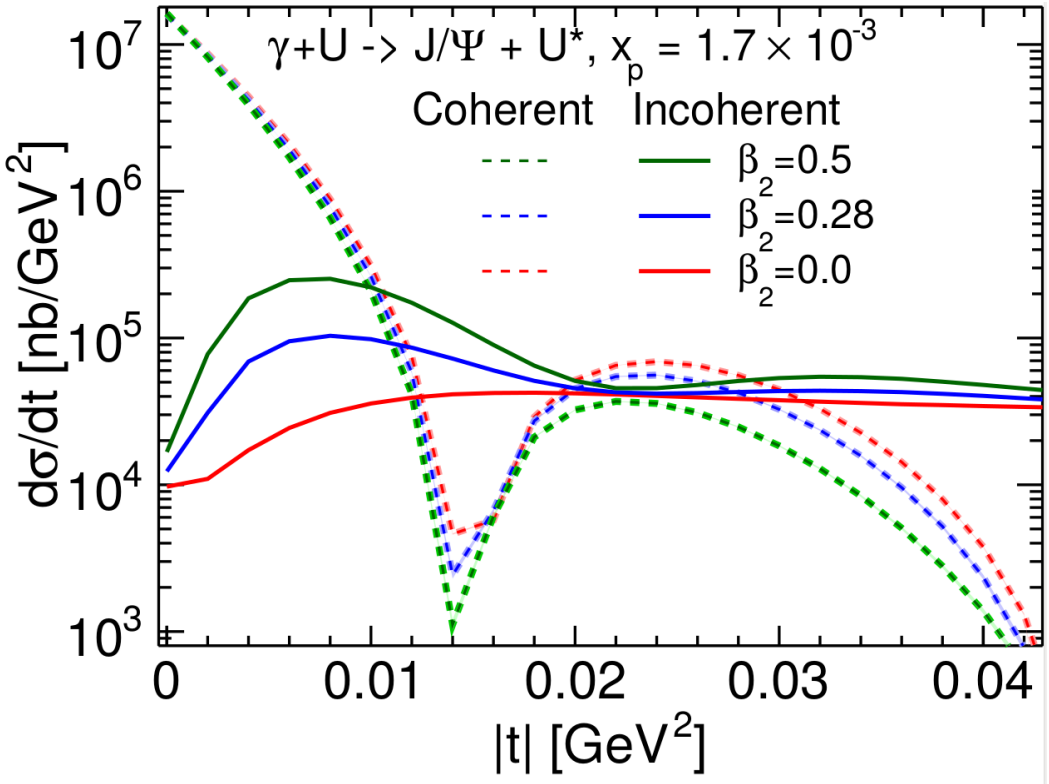

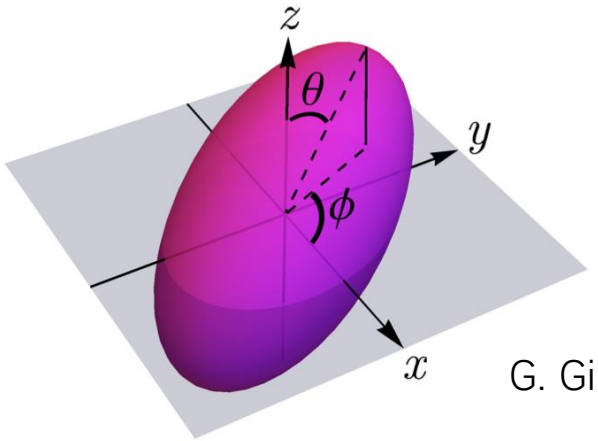

G. Giacalone, arXiv: 2004.14463

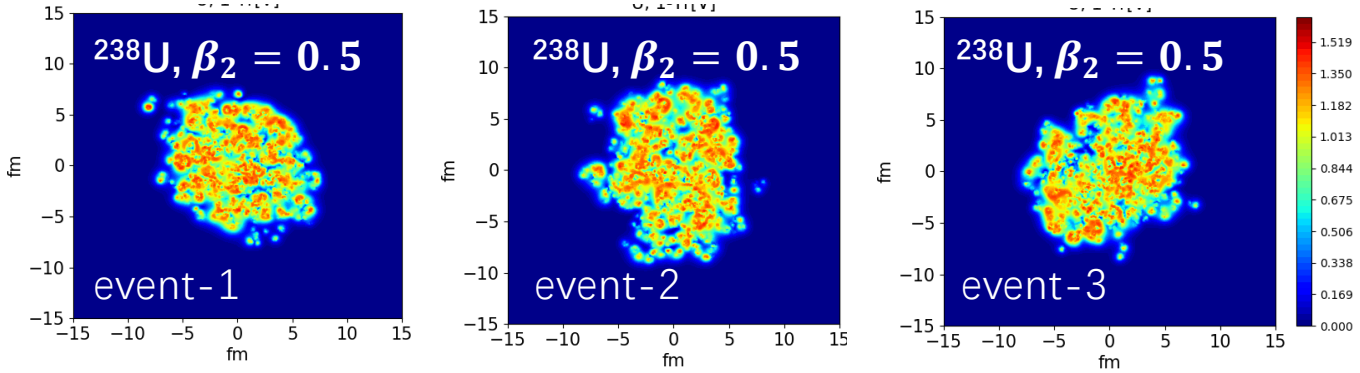

- With $\beta > 0$, the configurations projected onto x-y plane have great fluctuations.
- β_2 quadrupole deformation of the nucleus affects incoherent cross section at small|t|(large length scales) and provides direct information on the nuclear structure at small x.

H.Mantysaari, B.Schenke, C. Shen and W. Zhao, in progress.

β_2, β_3, and β_4

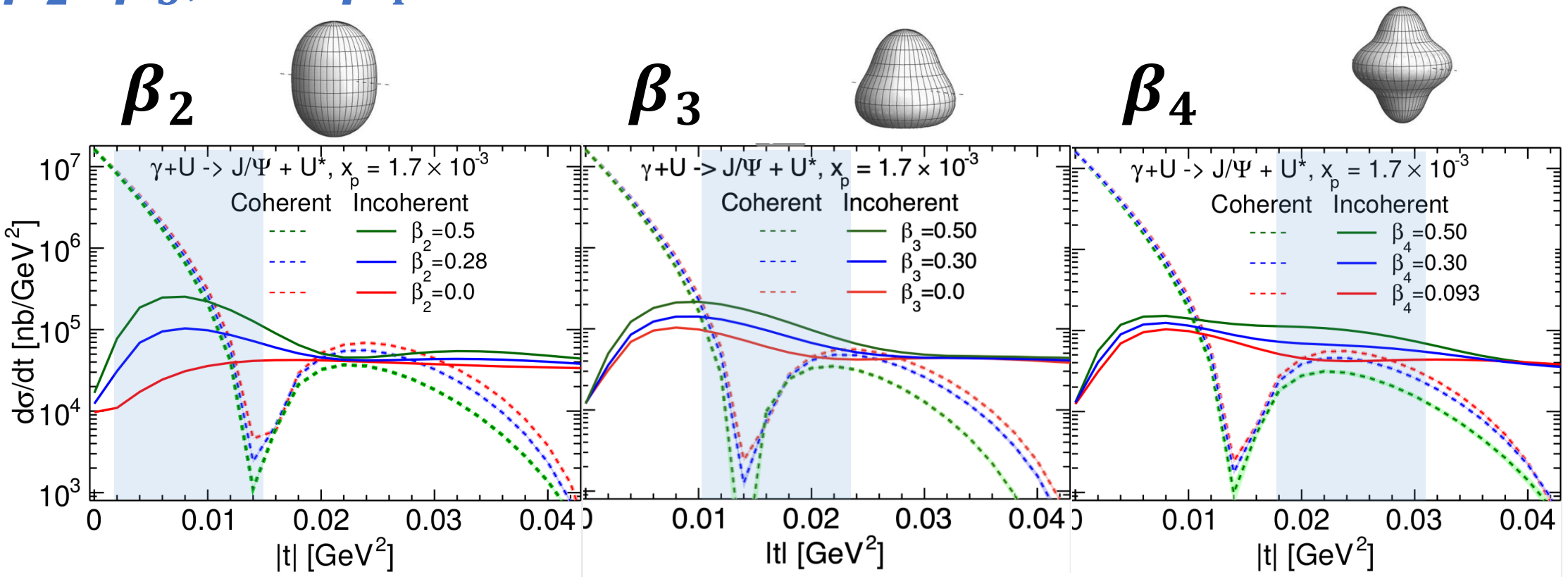

- β_2 , β_3 and β_4 manifest themselves at different |t| regions (different length scales).
- Different values of deformations don't affect the location of the first minimum of the coherent cross sections ($t_{first\ dip} \sim 1/R^2$). $\frac{d\sigma^{\gamma^* p \to Vp}}{dt} \sim e^{-B_p|t|}$,
- In the future, we will train the emulator with diffractive results. Then use trained emulator to predict the Woods-Saxon deformation parameters.

H.Mantysaari, B.Schenke, C. Shen and W. Zhao, in progress.

"See" sub-nucleon structures

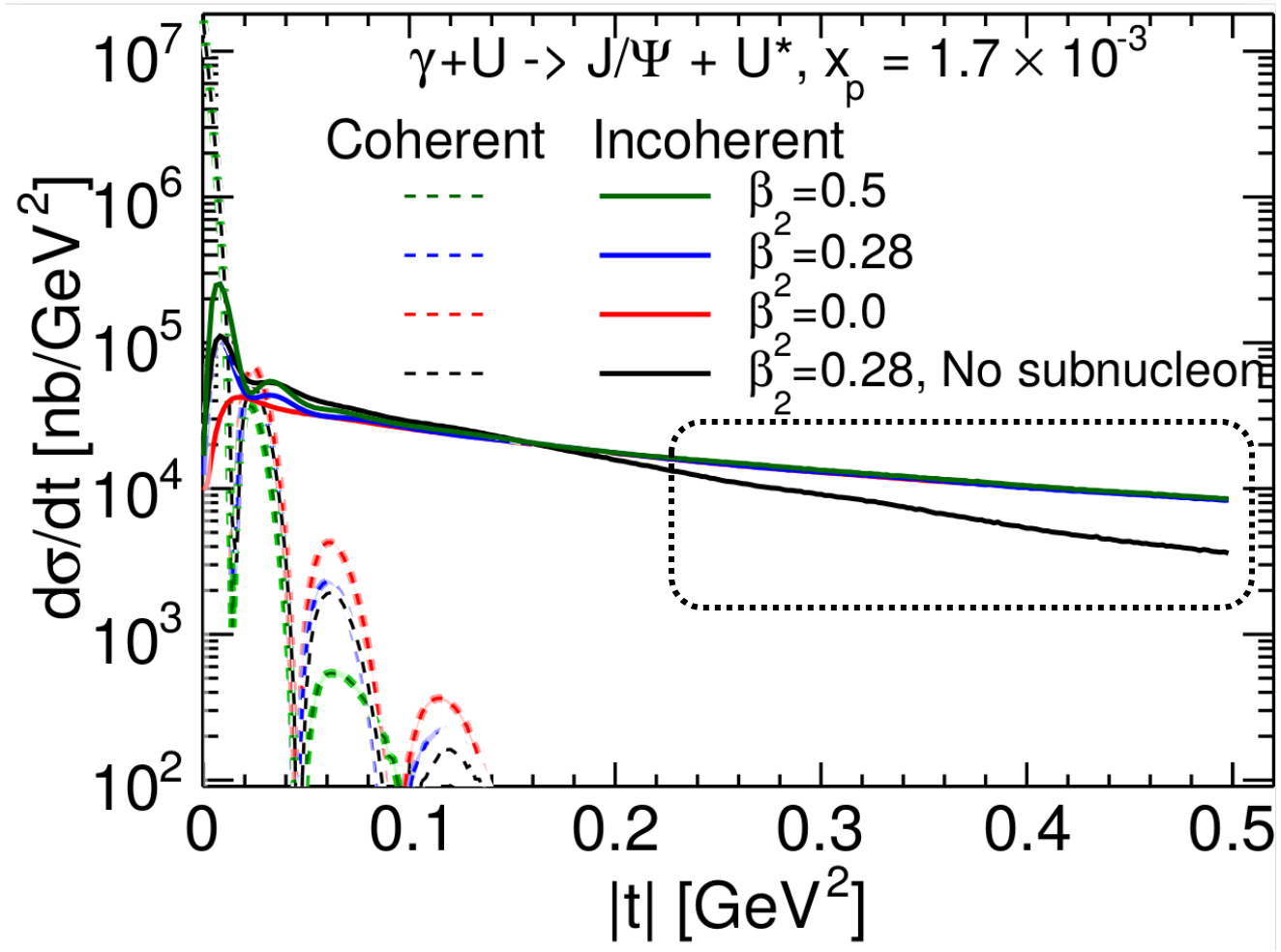

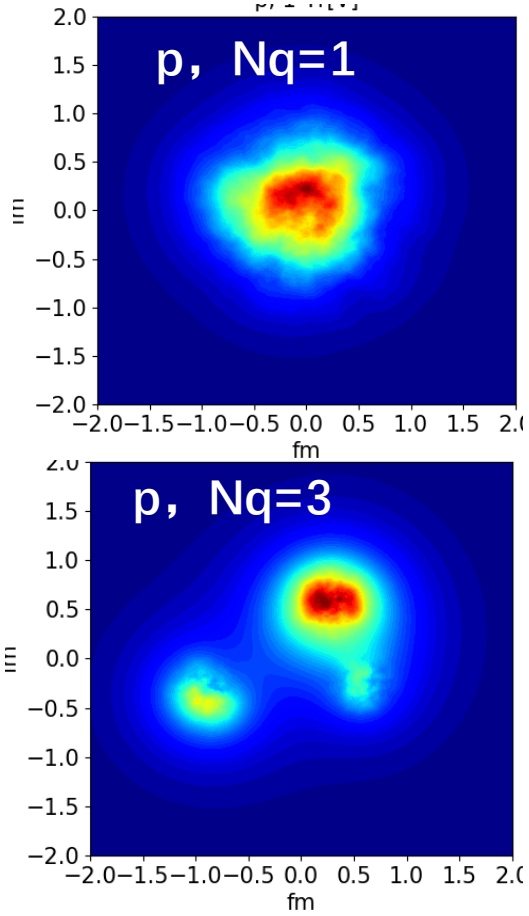

- High |t| region of gamma + A incoherent cross section probes sub-nucleon structures.

H.Mantysaari, B.Schenke, C. Shen and W. Zhao, Phys. Lett. B 833 (2022), 137348.
H.Mantysaari, B.Schenke, C. Shen and W. Zhao, in progress.

JIMWLK evolution to smaller xp

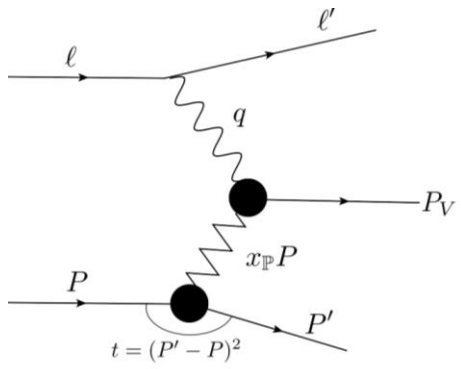

$$x_{\mathbb{P}} \equiv \frac{(P-P')\cdot q}{P\cdot q}$$

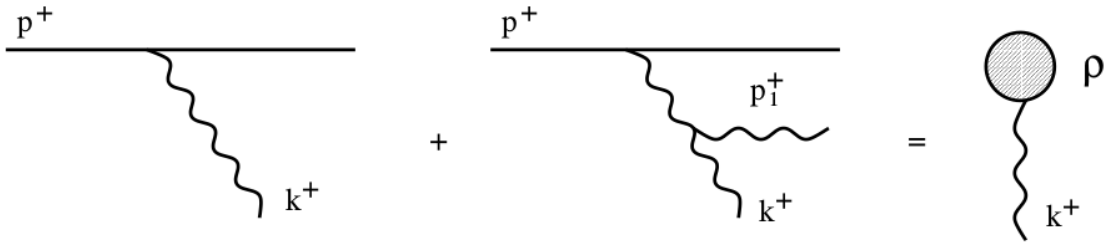

JIMWLK evolution:

1. Evolve the Wilson lines with energy (or rapidity) according to the Langevin equation.
2. Assuming the random noise is Gaussian and local in coordinates, color, and rapidity.

(More details in the back-up.)

- Absorb the quantum fluctuations in the middle x range into the color sources.

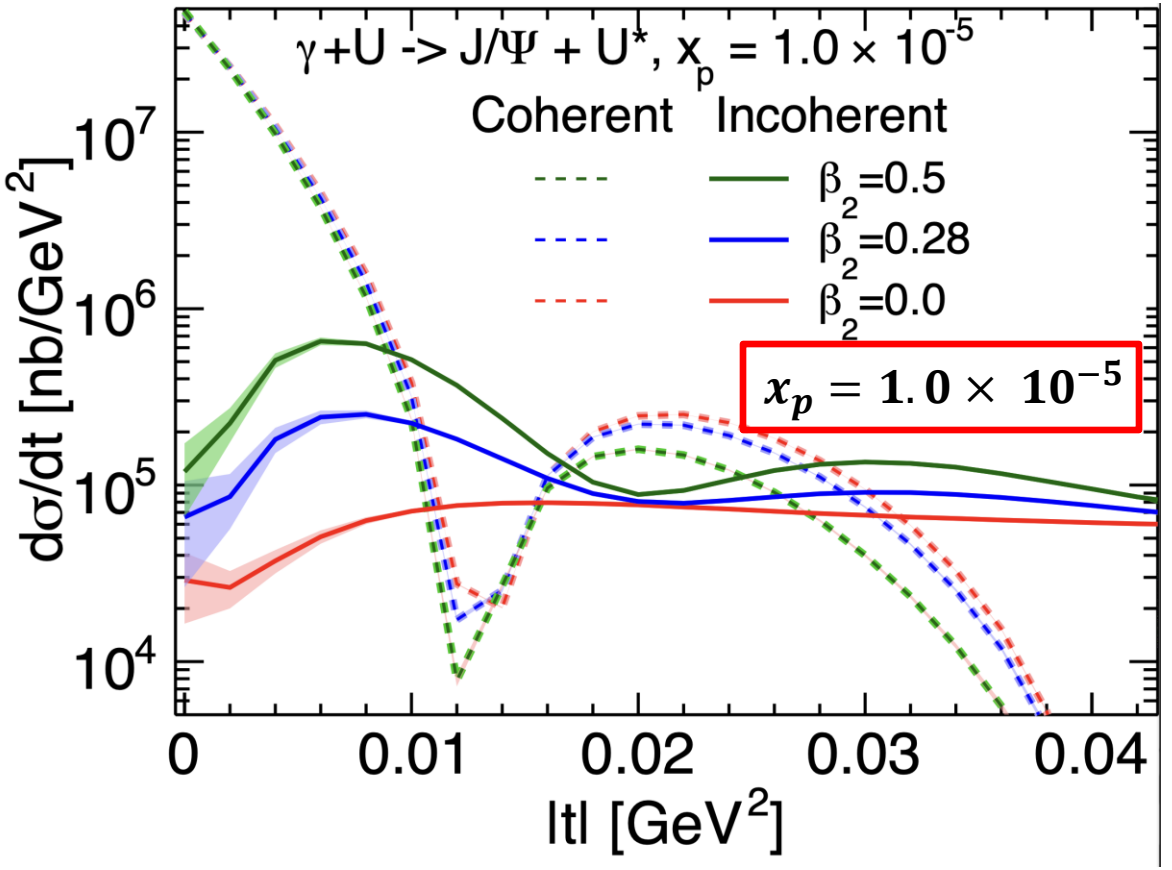

- JIMWLK evolution doesn't wash out this effects.

H.Mantysaari, B.Schenke, C. Shen and W. Zhao, in progress.
H.Mantysaari, B.Schenke PRD, 98, 034013.
T. Lappi and H. Mantysaari, EPJC 73, 2307 (2013).
Yuri V. Kovchegov, QUANTUM CHROMODYNAMICS A T HIGH ENERGY

JIMWLK evolution to smaller xp

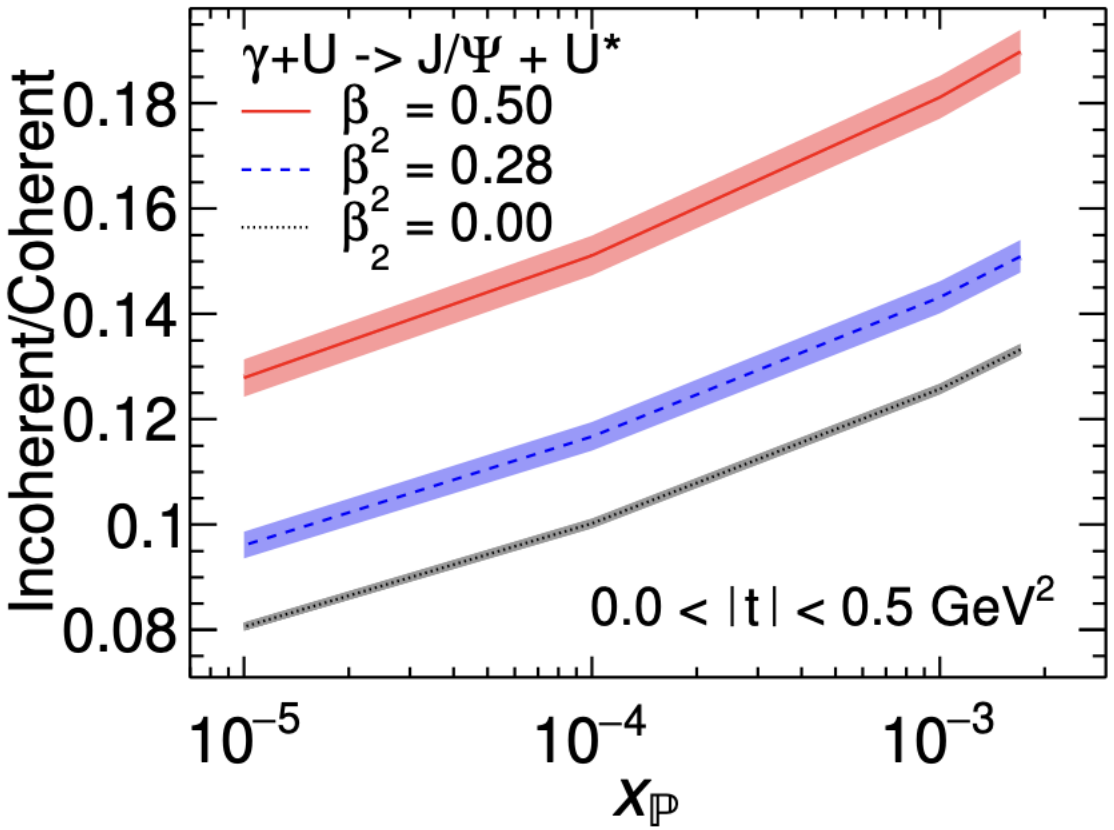

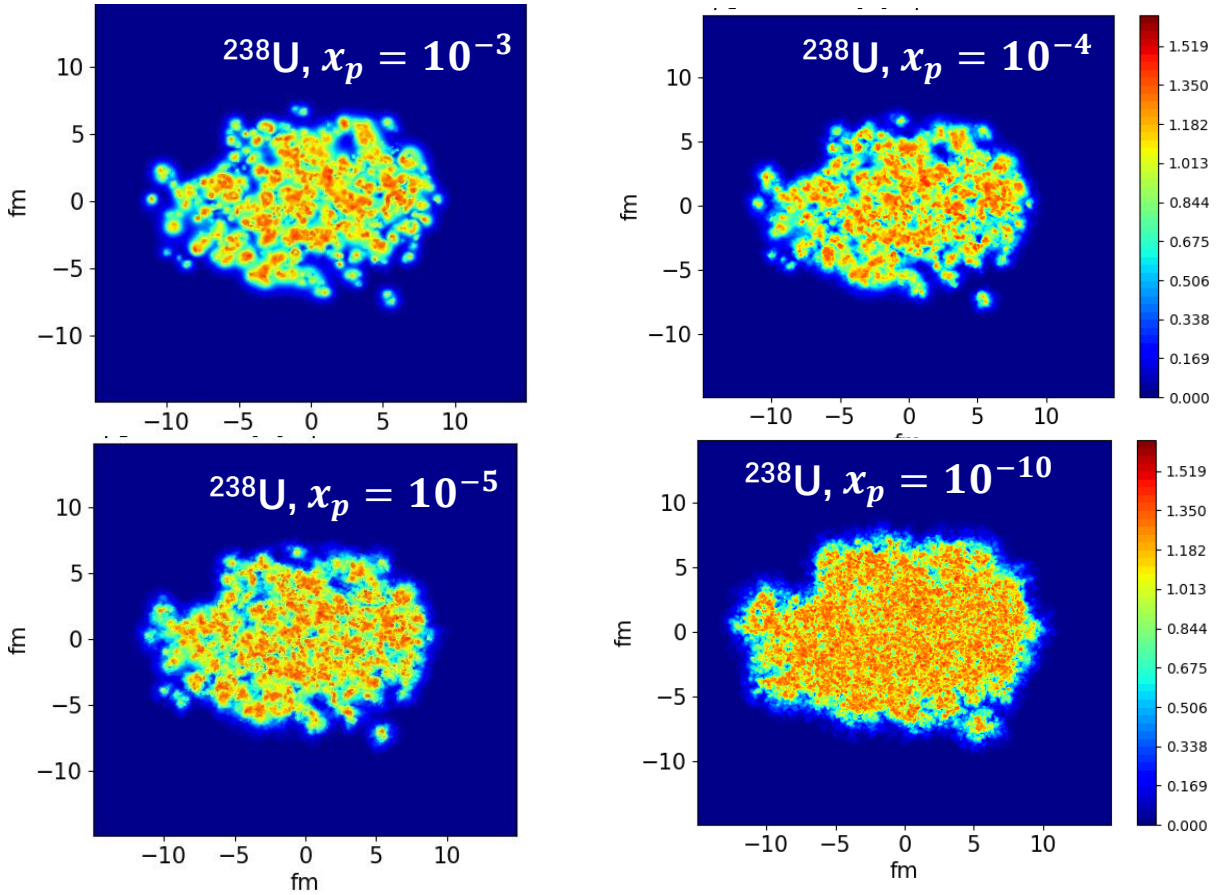

- Incoherent-to-coherent ratio effectively suppresses model uncertainties from wave functions.
- At smaller x_p, nucleon is smoother, reduces the fluctuations, decreases Incoherent-to-coherent ratio.
- JIMWLK evolution doesn't wash out difference between different β_2 (β_2 controls overall shape).

H.Mantysaari, B.Schenke, C. Shen and W. Zhao, in progress.
H.Mantysaari, B.Schenke PRD, 98, 034013.

Probing ^{20}Ne and ^{16}O

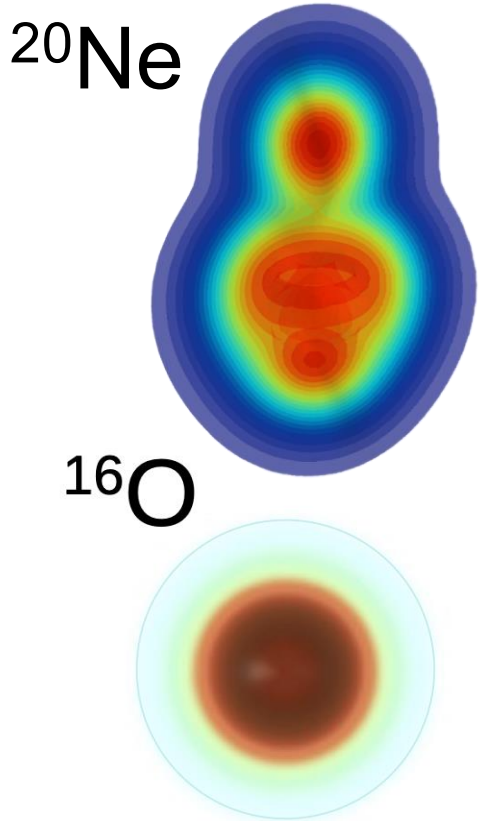

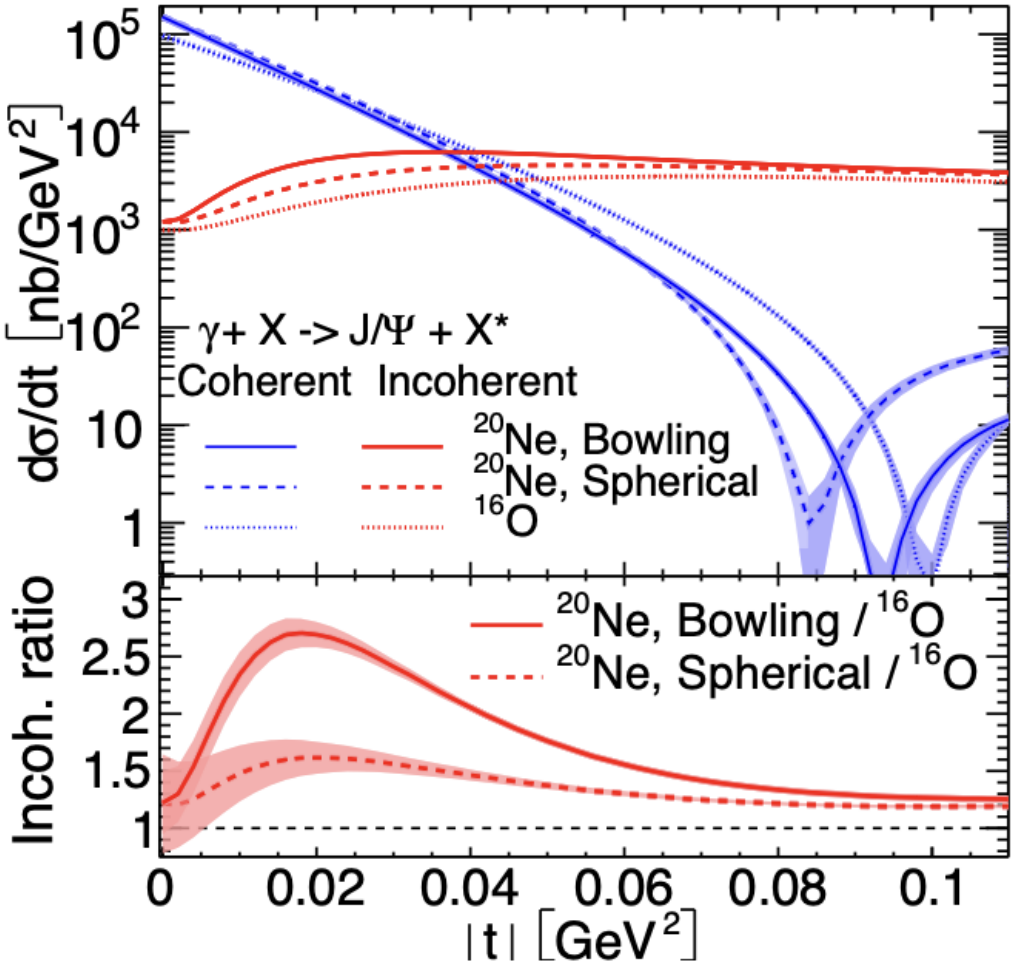

Nucleon density distribution is taken from G. Giacalone.

- Incoherent cross section at small |t| captures the deformation of the ^{20}Ne.
- Significant difference between ^{20}Ne and ^{16}O diffractive cross sections is observed.

H.Mantysaari, B.Schenke, C. Shen and W. Zhao, in progress.

Probing isobar, Ru/Zr

system to run	R_0 (fm)	a_0 (fm)	β_2	β_3	γ (°)	dmin(fm)
Case1 (^{96}Ru+^{96}Ru) [full ^{96}Ru]	5.09	0.46	0.16	0	30	0.0
Case2 (^{96}Ru+^{96}Ru)	5.09	0.46	0.16	0	0	0.9
Case3 (^{96}Ru+^{96}Ru)	5.09	0.46	0.16	0.20	0	0.9
Case4 (^{96}Ru+^{96}Ru)	5.09	0.46	0.06	0.20	0	0.9
Case5 (^{96}Ru+^{96}Ru)	5.09	0.52	0.06	0.20	0	0.9
Case6 (^{96}Zr+^{96}Zr) [full ^{96}Zr]	5.02	0.52	0.06	0.20	0	0.9

$$R(\Theta,\Phi) = R_0\left[1+\beta_2\left(\cos\gamma Y_{20}(\Theta)+\sin\gamma Y_{22}(\Theta,\Phi)\right)+\beta_3 Y_{30}(\Theta)+\beta_4 Y_{40}(\Theta)\right]$$

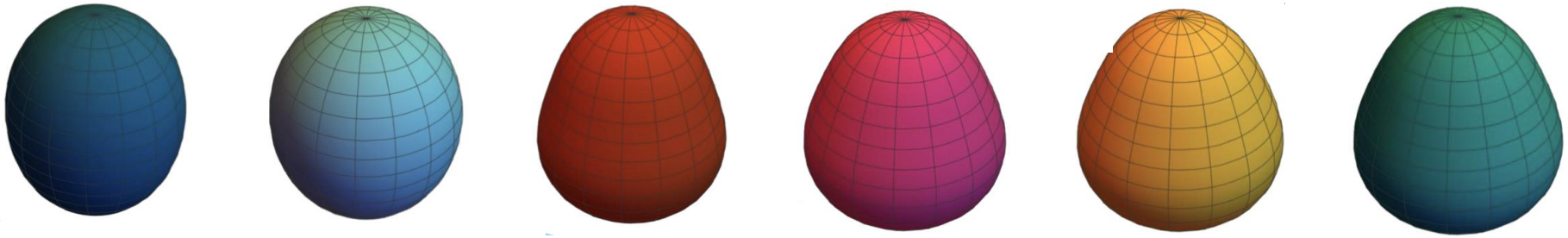

case1 case2 case3 case4 case5 case6

- Impose a minimal distance, dmin, between nucleons.

Taken from Willian Matioli Serenone's slide.

- When a nucleon is added and violates the minimum distance criterion with one or more already sampled nucleons, we resample its azimuthal angle ϕ to keep the distributions of radial distances and polar angles unchanged. ($\gamma \neq 0$, dmin = 0.0 fm)

J. S. Moreland, J. E. Bernhard and S. A. Bass, Phys. Rev. C 92 (2015) no.1, 011901.

Probing isobar, Ru/Zr

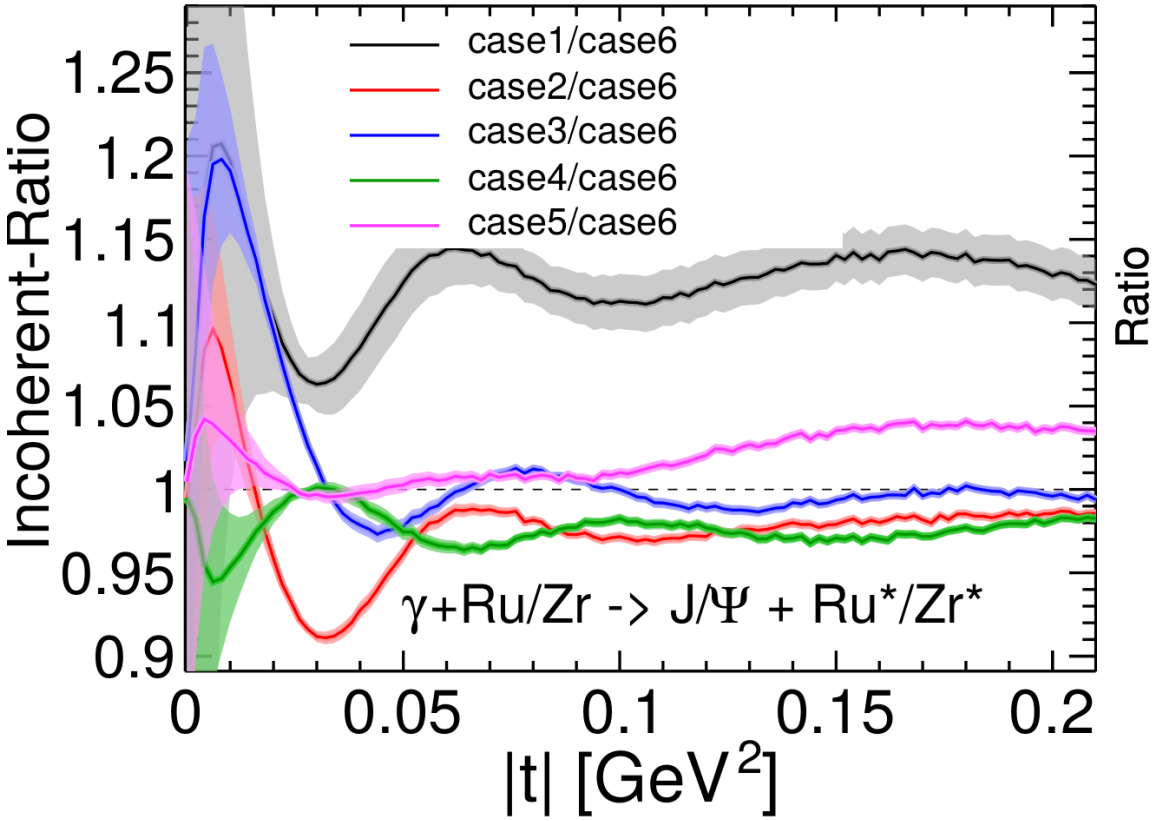

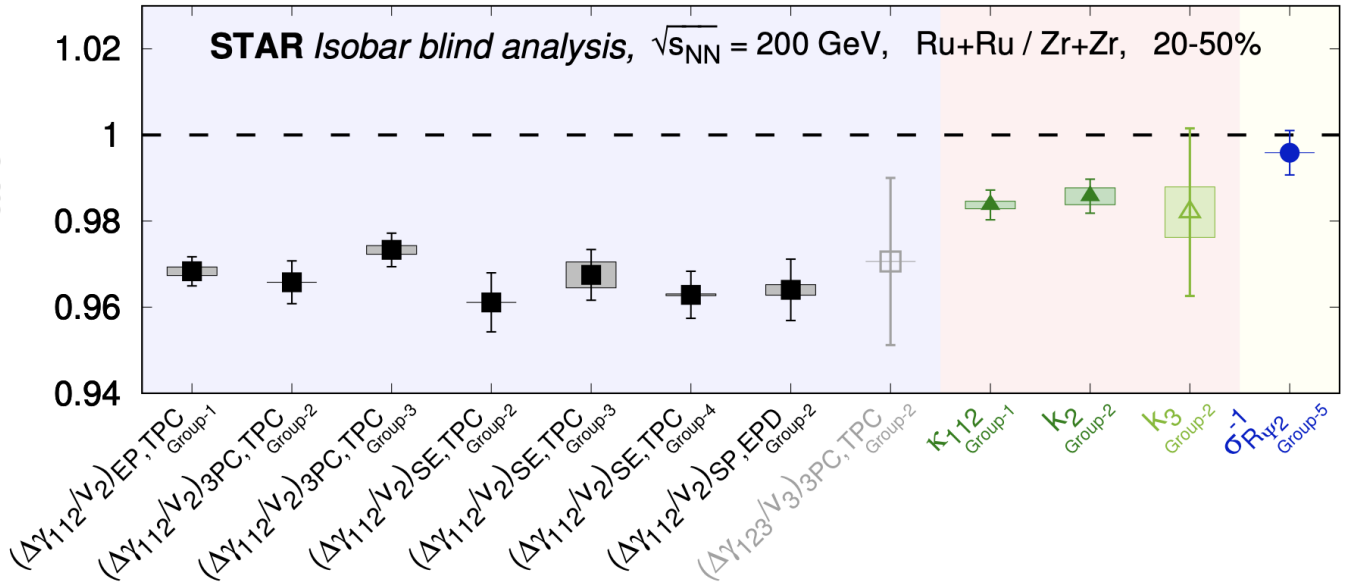

STAR, Phys. Rev. C 105 (2022) no.1, 014901.

- Differences of incoherent J/Ψ productions cross section between case2 -- case6 are within 5%.
- The difference between case1 and others mainly comes from dmin.

H.Mantysaari, B.Schenke, C. Shen and W. Zhao, in progress.

Summary

- We perform the first Bayesian analysis to constrain the proton shape fluctuations from diffractive J/Ψ data at HERA.
- Diffractive vector meson production is sensitive to average nuclear shape and fluctuations!
- JIMWLK evolution doesn't wash out this effect.
- Outlook
  1. Global analysis of HERA + LHC flow data.
  2. Train the emulator with diffractive results. Then use trained emulator predict the Woods-Saxon deformation parameters.

Thanks for Your Attentions!

Back Up

Diffractive vector meson production

High energy factorization:

1. $\gamma^* \to q\bar{q}$ splitting, wave function $\Psi^{\gamma}(r, Q^2, z)$
2. $q\bar{q}$ dipole scatters elastically
3. $q\bar{q} \to J/\Psi$, wave function $\Psi^{V}(r, Q^2, z)$

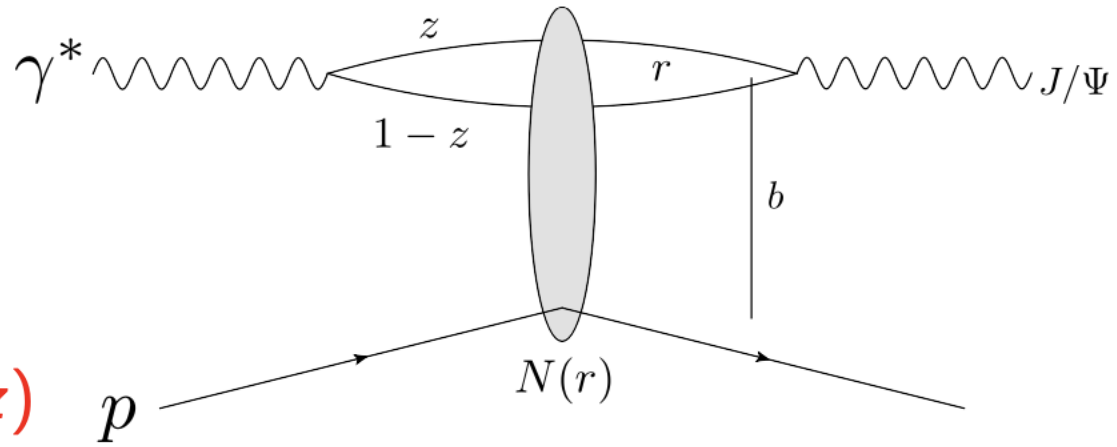

Diffractive scattering amplitude

Theoretically: no net color transfer

$$\mathcal{A}^{\gamma^* p \to Vp} \sim \int \mathrm{d}^2 b \mathrm{d}z \mathrm{d}^2 r \Psi^{\gamma *} \Psi^{V}(r, z, Q^2) \mathbf{e}^{-\mathbf{ib}\cdot\boldsymbol{\Delta}} N(r, x, b)$$

Impact parameter, b, is the Fourier conjugate of the momentum transfer, $\Delta \approx \sqrt{-t}$

$N(\mathbf{r}_T, \mathbf{b}_T, x) = 1 - \exp\left(-\mathbf{r}_T{}^2 F(\mathbf{r}_T, x) T_p(\mathbf{b}_T)\right)$ **accesses to the spatial structure ($T_{p/A}$)**

$F(\mathbf{r}_T, x) = \frac{\pi^2}{2N_c} \alpha_s(\mu^2) x g(x, \mu^2)$. $xg(x, \mu^2)$, gluon density at x and scale μ^2 $(\mu^2 \sim \mu_0^2 + 1/r_T^2)$.

Miettinen, Pumplin, PRD 18, 1978; Caldwell, Kowalski, 0909.1254; Mäntysaari, Schenke, 1603.04349; Mäntysaari, 2001.10705

MAP

Parameter	Description	$N_q = 9$	$N_q = 3$
m [GeV]	Infrared regulator	0.780	0.246
B_{qc} [GeV^{-2}]	Proton size	3.98	4.45
B_q [GeV^{-2}]	Hot spot size	0.594	0.346
σ	Magnitude of Q_s fluctuations	0.932	0.563
$Q_s/(g^2\mu)$	$Q_s \Rightarrow$ color charge density	0.492	0.747
$d_{q,\mathrm{Min}}$ [fm]	Min hot spot distance	0.265	0.254
N_q	Number of hot spots	3	9
S	Hydro normalization	0.1135	0.235

JIMWLK

$$V_{ij}(\vec{x}_T) = \mathscr{P}\left(ig \int_{-\infty}^{\infty} A^{+,c}(z^-, \vec{x}_T)\, t^c_{ij}\, dz^- \right)$$

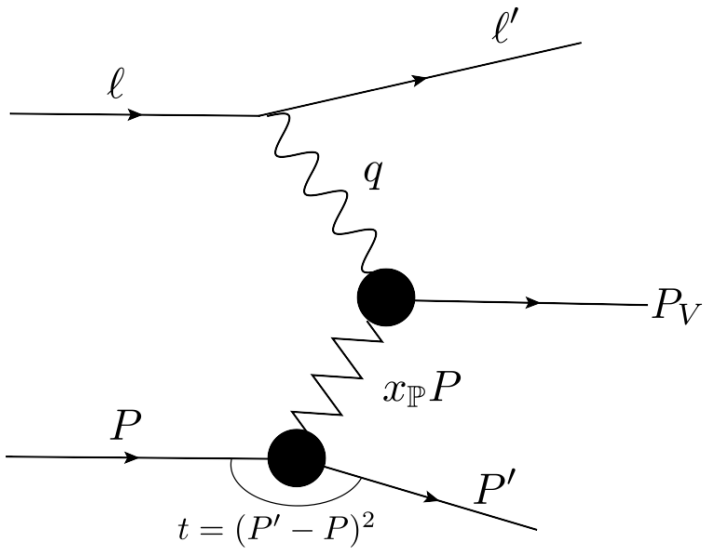

Evolve the Wilson lines according to the Langevin equation

$$\frac{\mathrm{d}}{\mathrm{d}y} V_{\mathbf{x}} = V_{\mathbf{x}}(it^a)\left[\int \mathrm{d}^2\mathbf{z}\,\varepsilon^{ab,i}_{\mathbf{x},\mathbf{z}}\,\xi_{\mathbf{z}}(y)^b_i + \sigma^a_{\mathbf{x}}\right].$$

The deterministic drift term is

$$\sigma^a_{\mathbf{x}} = -i\frac{\alpha_s}{2\pi^2}\int \mathrm{d}^2\mathbf{z} S_{\mathbf{x}-\mathbf{z}} \mathrm{Tr}[T^a U^\dagger_{\mathbf{x}} U_{\mathbf{z}}], \quad S_{\mathbf{x}} = 1/\mathbf{x}^2$$

The random noise is Gaussian and local in coordinates, color, and rapidity with expectation value zero and

$$\langle \xi^a_{\mathbf{x},i}(y)\xi^b_{\mathbf{y},j}(y')\rangle = \delta^{ab}\delta^{ij}\delta^{(2)}_{\mathbf{xy}}\delta(y-y').$$

The coefficient of the noise in the stochastic term is

$$\varepsilon^{ab,i}_{\mathbf{x},\mathbf{z}} = \left(\frac{\alpha_s}{\pi}\right)^{1/2} K^i_{\mathbf{x}-\mathbf{z}}[1 - U^\dagger_{\mathbf{x}} U_{\mathbf{z}}]^{ab}, \quad K^i_{\mathbf{x}} = \frac{x^i}{\mathbf{x}^2}.$$

H.Mantysaari, B.Schenke PRD, 98, 034013.

JIMWLK

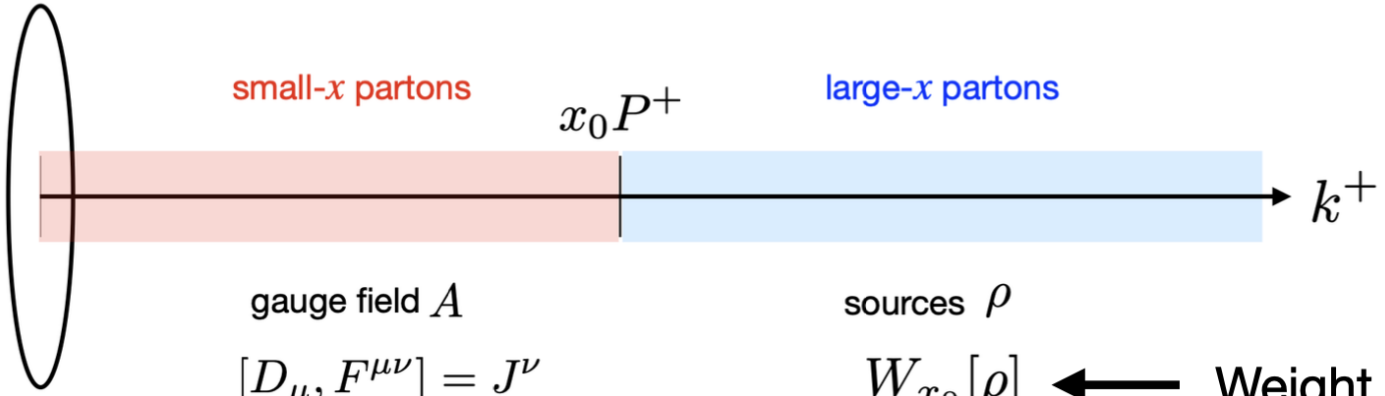

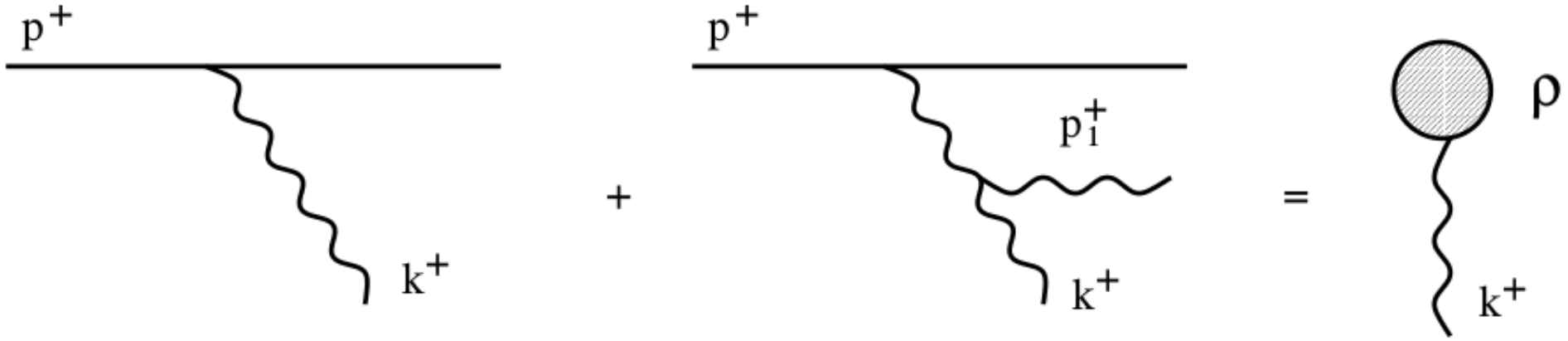

$$\frac{\partial W_\tau[\alpha]}{\partial \tau} = \frac{1}{2}\int_{\boldsymbol{x},\boldsymbol{y}} \frac{\delta^2}{\delta\alpha_\tau^a(\boldsymbol{x})\delta\alpha_\tau^b(\boldsymbol{y})}\left[W_\tau \chi_{xy}^{ab}\right] - \int_{\boldsymbol{x}} \frac{\delta}{\delta\alpha_\tau^a(\boldsymbol{x})}\left[W_\tau \sigma_x^a\right],$$

Wilson lines

$$V_{ij}(\vec{x}_T) = \mathscr{P}\left(ig \int_{-\infty}^{\infty} A^{+,c}(z^-, \vec{x}_T)\, t^c_{ij}\, dz^- \right)$$

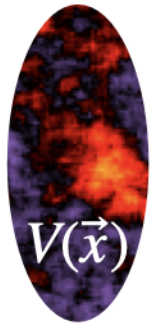

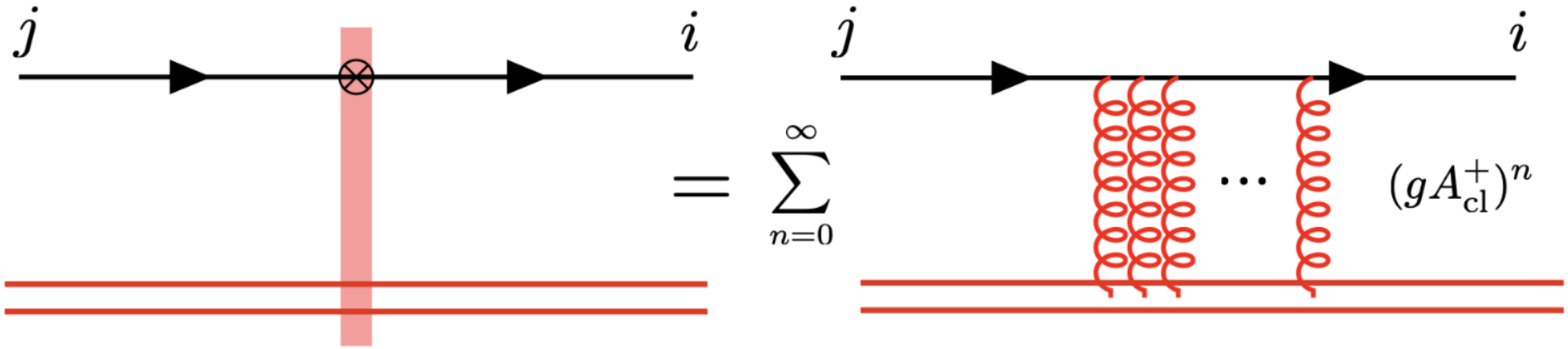

MULTIPLE INTERACTIONS NEED TO BE RESUMMED, BECAUSE $A^+ \sim 1/g$

Wilson lines

$$\mathcal{A}^{\gamma^* p\to Vp} \sim \int \mathrm{d}^2b\mathrm{d}z\mathrm{d}^2r\Psi^{\gamma^*}\Psi^{V}(r,z,Q^2)\mathrm{e}^{-\mathrm{i}\mathbf{b}\cdot\mathbf{\Delta}}N(r,x,b)$$

$$N_\Omega(\mathbf{r}_\perp,\mathbf{b}_\perp,x_{\mathbb{P}}) = 1-\frac{1}{N_c}\,\mathrm{tr}\left[V\left(\mathbf{b}_\perp+\frac{\mathbf{r}_\perp}{2}\right)V^\dagger\left(\mathbf{b}_\perp-\frac{\mathbf{r}_\perp}{2}\right)\right].$$

$$V(\mathbf{x}_\perp) = \mathrm{P}_-\left\{\exp\left(-ig\int_{-\infty}^{\infty}\mathrm{d}z^-\,\frac{\rho^a(x^-,\mathbf{x}_\perp)t^a}{\boldsymbol{\nabla}^2-m^2}\right)\right\}$$

$$g^2\left\langle\rho^a(x^-,\mathbf{x}_\perp)\rho^b(y^-,\mathbf{y}_\perp)\right\rangle = g^4\lambda_A(x^-)\delta^{ab} \times\delta^{(2)}(\mathbf{x}_\perp-\mathbf{y}_\perp)\delta(x^--y^-)\,.$$

From the dipole amplitude $\mathcal{N}(x,\mathbf{r}_\perp,\mathbf{b}_\perp) = (d\sigma^p_{\mathrm{dip}}/d^2\mathbf{b}_\perp)(x,\mathbf{r}_\perp,\mathbf{b}_\perp)/2$ given by Eq. (1), we can extract a saturation scale $Q_s(x)$ by using the definition that $Q_s^2 = 2/R_s^2$, with R_s defined via $\mathcal{N}(x,R_s) = 1-\exp(-1/2)$. Note that $\mathcal{N}$ and Q_s also depend on the thickness function T_A

$\mu^2 = \int \mathrm{d}x^-\,\lambda_A(x^-)$, $\quad \dfrac{Q_s(\mathbf{x}_\perp)}{g^2\mu}$, is a free parameter

B. Schenke, C. Shen and P. Tribedy, Phys. Rev. C 102 (2020) no.4, 044905.
H.Mantysaari, B.Schenke, C. Shen and **W. Zhao**, Phys. Lett. B 833 (2022), 137348.

Universal Wilson lines

We use one framework to compute Wilson lines for a nucleus at a given energy.

This allows to directly constrain parameters (like hot spot sizes) using one process (e.g. in e+A or e+p) and employ the model for another (e.g. in A+A or p+A)

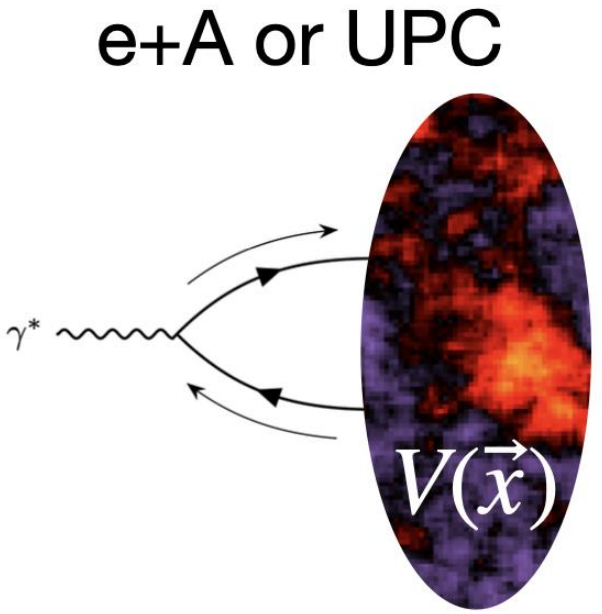

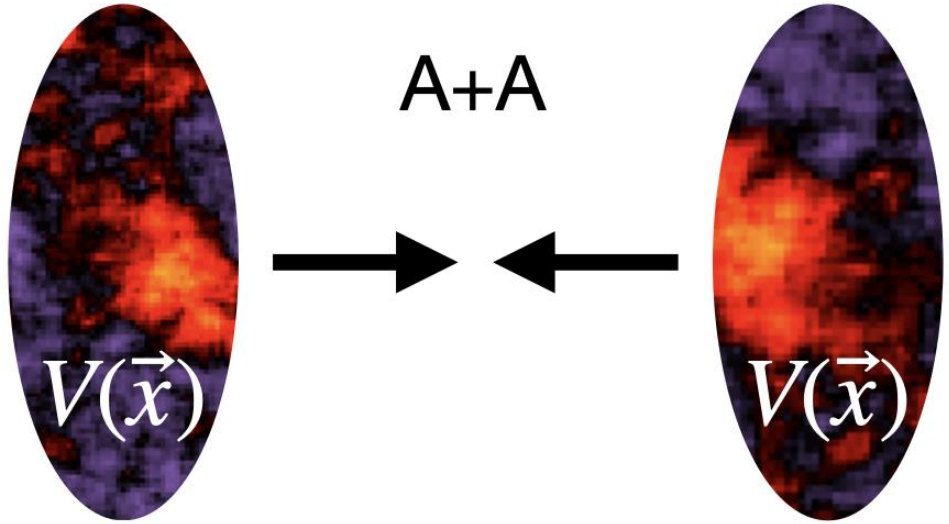

From Bjorn's slide

Color Glass Condensate (CGC): Sources and fields

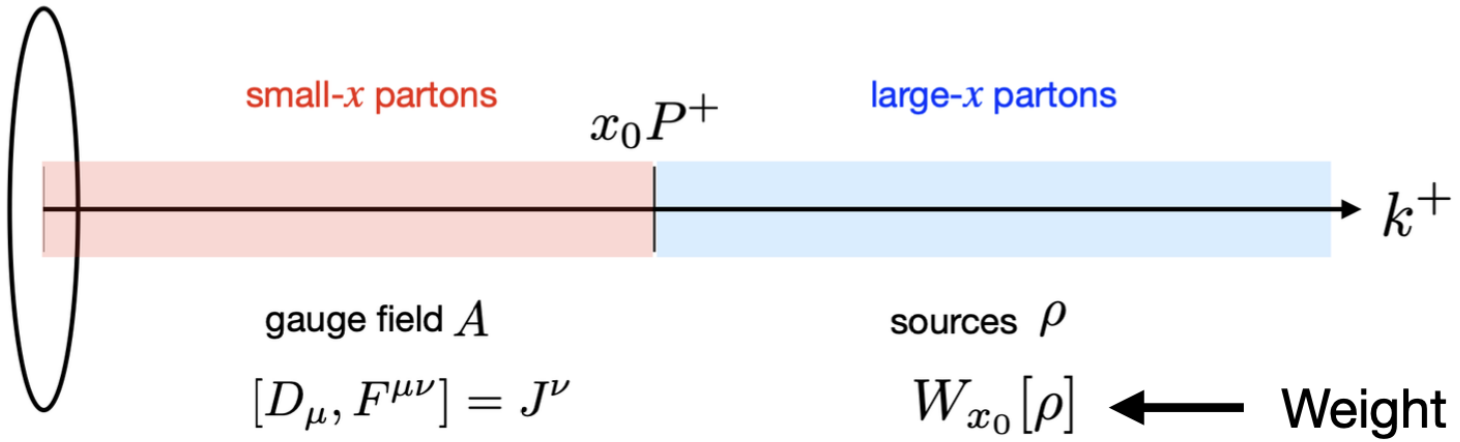

Two steps to compute expectation value of an observable $\mathcal{O}$:

1) Compute quantum expectation value $\mathcal{O}[\rho] = \langle \mathcal{O} \rangle_\rho$ for sources drawn from a given $W_{x_o}[\rho]$

2) Average over all possible configurations given the appropriate gauge invariant weight functional $W_{x_o}[\rho]$ (e.g. from McLerran Venugopalan model)

When $x \lesssim x_0$ the path integral $\langle \mathcal{O} \rangle_\rho$ is dominated by classical solution and we are done

For smaller x we need to do quantum evolution

From Bjorn's slide [4]

Location of the first dip

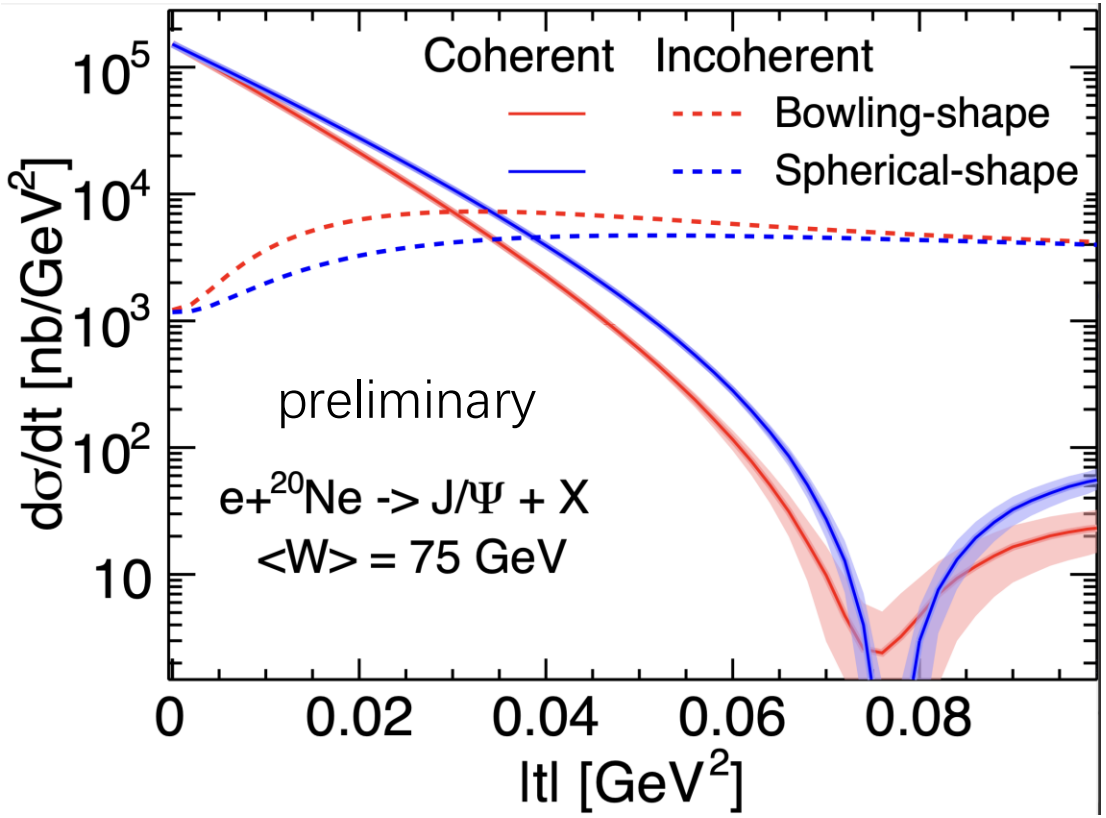

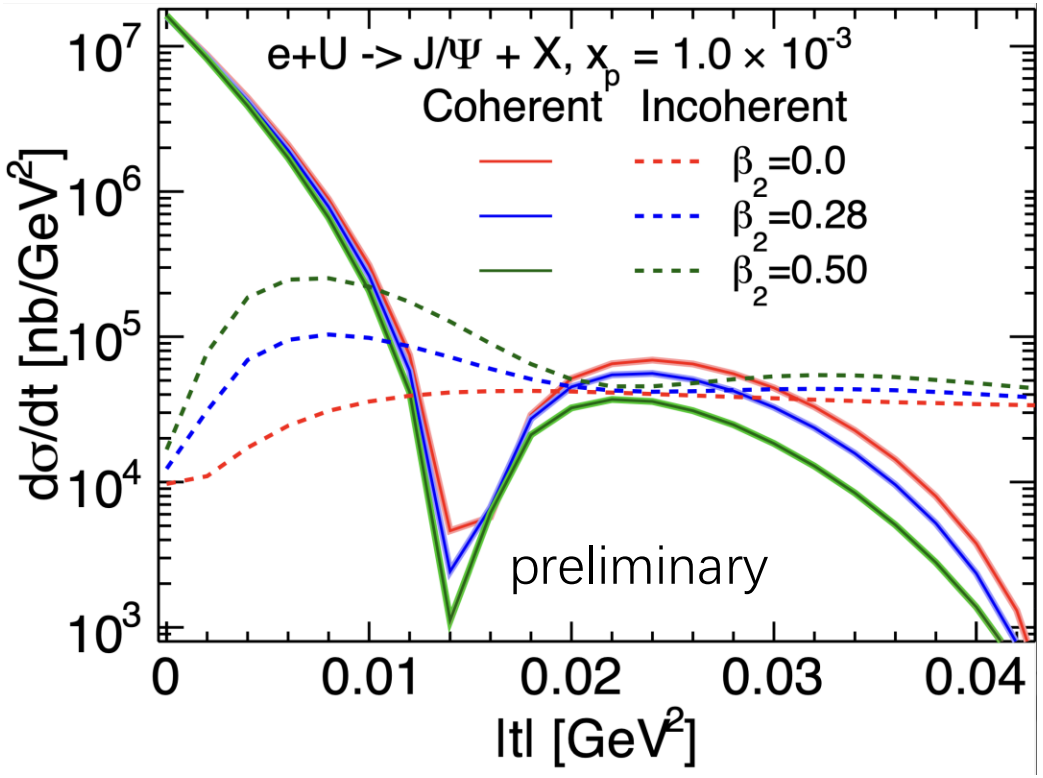

$$\frac{\mathrm{d}\sigma^{\gamma^* p\to Vp}}{\mathrm{d}t} \sim e^{-B_p|t|}, \qquad T_p(\mathbf{b}_T) = \frac{1}{2\pi B_p} e^{-\mathbf{b}_T{}^2/(2B_p)}.$$

H.Mantysaari, B.Schenke, C. Shen and **W. Zhao**, in progress.

Wave functions

Forward photon wave functions (QED)

$$\Psi_{h\bar{h},\lambda=0}(r,z,Q) = e_f e\sqrt{N_c}\,\delta_{h,-\bar{h}}\,2Qz(1-z)\,\frac{K_0(\epsilon r)}{2\pi},$$

$$\Psi_{h\bar{h},\lambda=\pm1}(r,z,Q) = \pm e_f e\sqrt{2N_c}\,\left\{\mathrm{i}e^{\pm\mathrm{i}\theta_r}[z\delta_{h,\pm}\delta_{\bar{h},\mp} - (1-z)\delta_{h,\mp}\delta_{\bar{h},\pm}]\partial_r + m_f\delta_{h,\pm}\delta_{\bar{h},\pm}\right\}\,\frac{K_0(\epsilon r)}{2\pi},$$

Vector meson: Boosted Gaussian (Non-perturbative)

$$\phi_{T,L}(r,z) = \mathcal{N}_{T,L}z(1-z)\exp\left(-\frac{m_f^2\mathcal{R}^2}{8z(1-z)} - \frac{2z(1-z)r^2}{\mathcal{R}^2} + \frac{m_f^2\mathcal{R}^2}{2}\right)$$

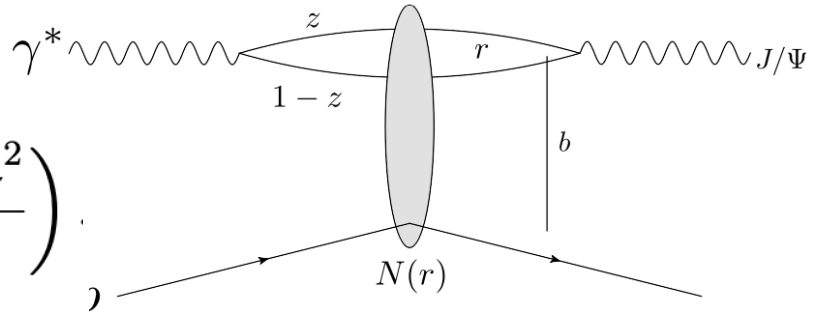

Meson	M_V/GeV	f_V	m_f/GeV	$\mathcal{N}_T$	$\mathcal{N}_L$	$\mathcal{R}^2$/GeV^{-2}	$f_{V,T}$
J/ψ	3.097	0.274	1.4	0.578	0.575	2.3	0.307
ϕ	1.019	0.076	0.14	0.919	0.825	11.2	0.075
ρ	0.776	0.156	0.14	0.911	0.853	12.9	0.182

H. Kowalski, L. Motyka and G. Watt, Phys. Rev. D 74 (2006), 074016.

Different vector meson's wave functions

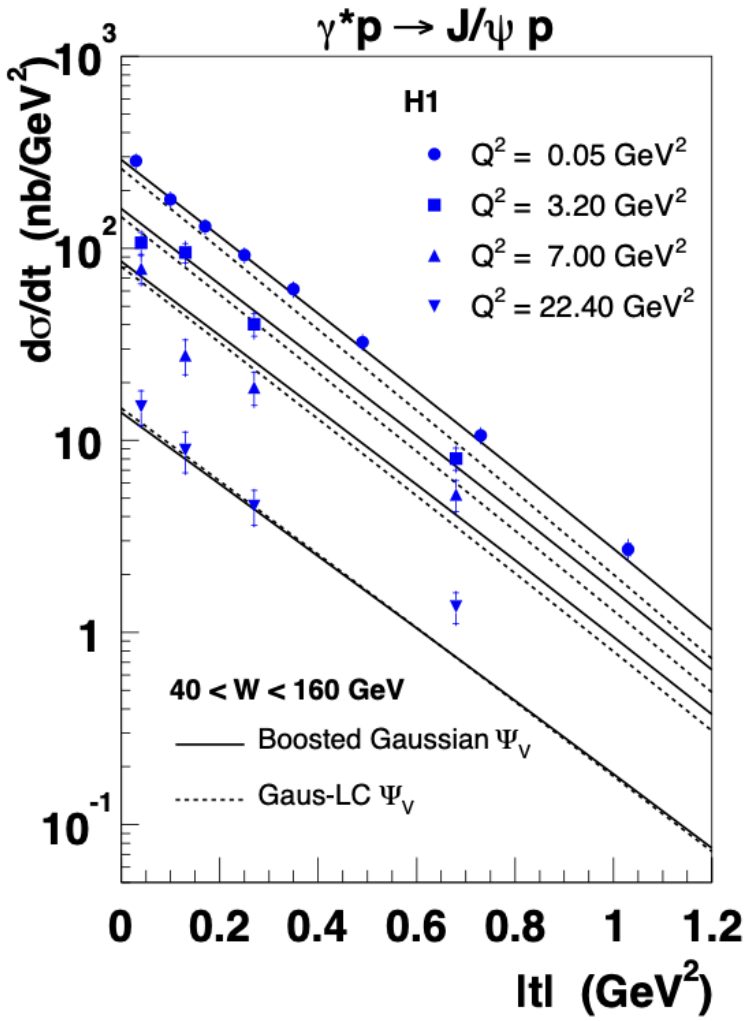

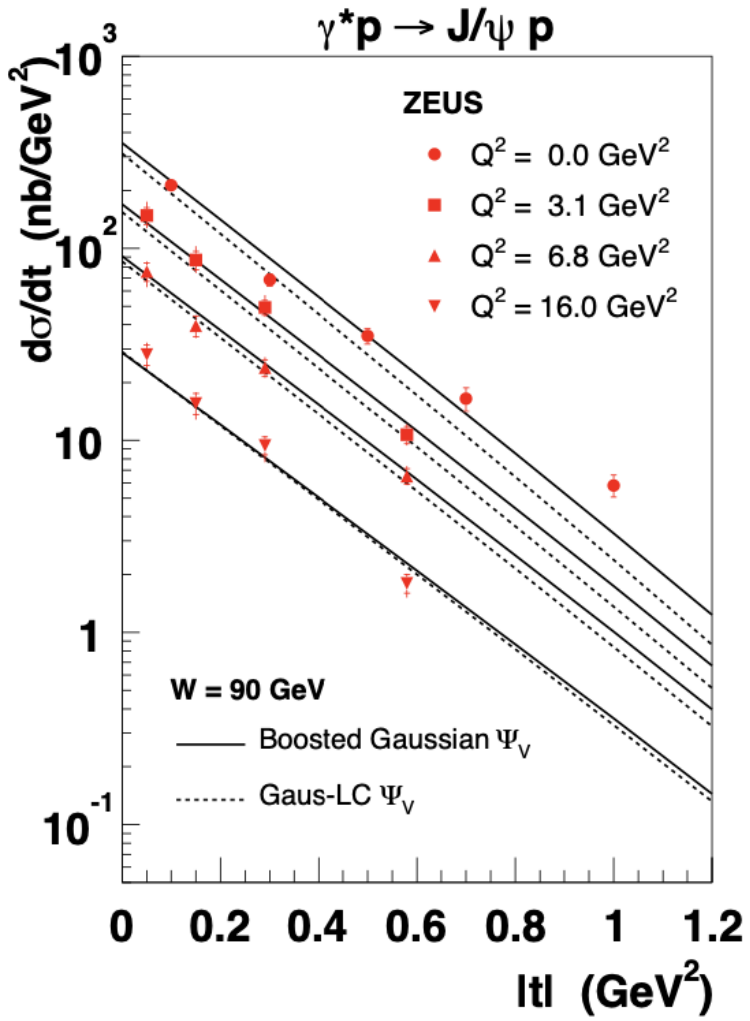

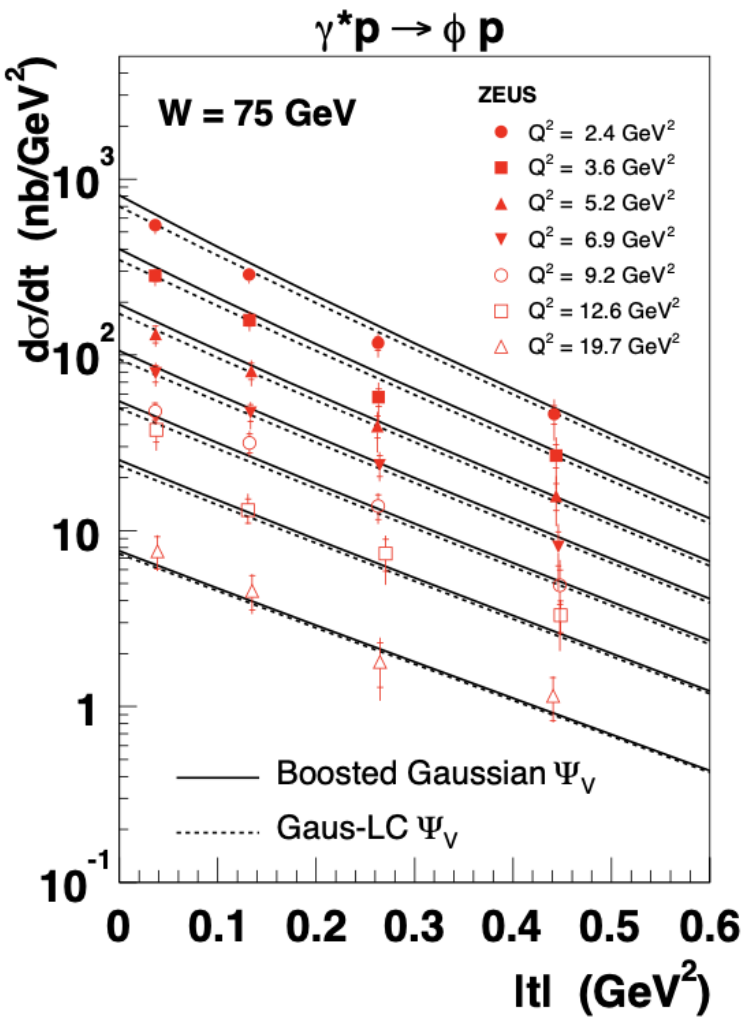

H. Kowalski, L. Motyka and G. Watt, Phys. Rev. D 74, (2006), 074016.

Virtuality dependent PDF

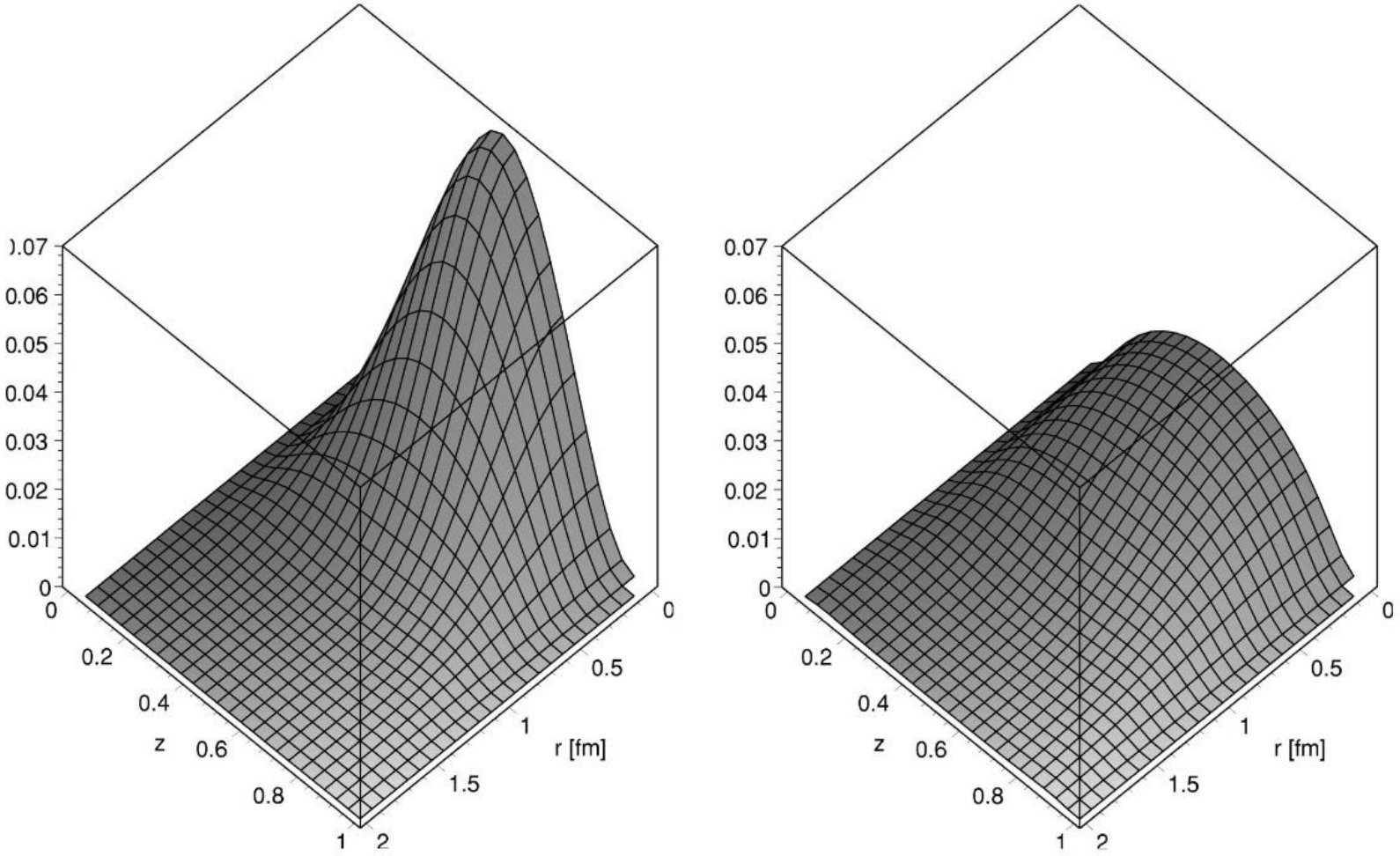

FIG. 6. The ρ wave functions $|\Psi^L|^2$ (left) and $|\Psi^T|^2$ (right) in the boosted Gaussian model with the quark mass used in the FKS dipole model.

J. R. Forshaw, R. Sandapen and G. Shaw, Phys. Rev. D 69, 094013 (2004).